

1507

237
2/13/79

Ln. 2187

JANUARY 1979

PPPL-1507
UC-20b,r

CHARGE EXCHANGE ION TEMPERATURE
MEASUREMENTS DURING HIGH POWER
NEUTRAL BEAM INJECTION ON PLT

BY

S. S. MEDLEY AND S. L. DAVIS

**PLASMA PHYSICS
LABORATORY**



MASTER

**PRINCETON UNIVERSITY
PRINCETON, NEW JERSEY**

This work was supported by the U. S. Department of Energy
Contract No. EY-76-C-02-3073. Reproduction, translation,
publication, use and disposal, in whole or in part, by or
for the United States Government is permitted.

CRITICAL POINTS IN TEMPERATURE-MEASUREMENTS
IN A LOW-DENSITY NEUTRAL-BEAM INJECTION PLASMA

S. T. Medley and J. L. Davis

Plasma Physics Laboratory, Princeton University
Princeton, N. J. 08540

SYNOPSIS

A compilation and analysis of temperature-impurity temperature measurements obtained during recent experiments on the Princeton University tokamak, Princeton Plasma Physics Laboratory, are presented. For titanium-potted tungsten-coated carbon limiter (a ~ 5 cm), PFT produced ion temperatures up to 1.0 keV ($T_{i0} = 3.5 - 4.0$ keV) with 2.4 MW-level neutral deuterium injection into low-density hydrogen and deuterium plasmas. Over the parameter space ($P_{inj} = 0.7 - 1.6$ MW) and line-averaged electron density ($\bar{n}_e = 1.0 - 2.0 \times 10^{17} \text{ cm}^{-3}$) parameter space thus far explored, the ion temperature, in eV, T_{i0} , is found to scale according to the empirical relation $T_{i0} \text{ (eV)} = 4.2 \times 10^{-2} P_{inj} \text{ (MW)} / \bar{n}_e^{1/2} \text{ (cm}^{-3})$, where \bar{n}_e is the line-averaged electron density at low ion temperature.

I. INTRODUCTION

Charge exchange ion temperature results obtained during high power neutral beam heating experiments on PLT are reported. The measurements were obtained using a recently installed 5-channel analyzer¹ which provides mass resolved charge exchange distributions over a calibrated energy range of 0.75 - 40 keV. Although the system design provides capability for active, radially scanned measurements, this facility is not operational as yet. Over the reporting period, therefore, all charge exchange data are passive measurements with the analyzer viewing a horizontal minor diameter. Furthermore, the operation of PLT was characterized during this period by use of 40 cm radius water-cooled carbon limiters and titanium gettering of the torus. As discussed in a recent survey of beam heating results,² this mode of operation suppressed the high Z impurity level which is essential to attaining the strong beam heating observed

The heating experiments involved varying the injected beam power and target plasma density while maintaining other discharge conditions as invariant as possible. Most experiments used neutral deuterium injection into a hydrogen plasma ($D^0 \rightarrow H^+$), though some results using $H^0 \rightarrow D^+$ and $D^0 \rightarrow D^+$ were also obtained.

A brief review of the charge exchange data acquisition process is followed by a compilation of ion temperature measurements in Section II. The dependence of the ion temperature increase on beam power and plasma density is examined in Section III. This section also includes a preliminary analysis of the observed rise and fall times of the ion heating. Section IV presents a discussion of various effects relevant to both the interpretation of the charge exchange results as well as the aforementioned analysis. The last section summarizes the reported results.

II. CHARGE EXCHANGE MEASUREMENTS

A detailed description of the charge exchange data acquisition process is contained in an earlier report.¹ For present purposes, however, a brief review is deemed useful.

The analyzer detectors are channel electron multipliers (see Fig. 1) operated in the pulse counting mode. Signals from each of the five energy channels are processed in parallel. The channel electron multiplier pulses are conditioned by amplifier-discriminators and fed via coaxial cables into a multichannel scalar interfaced to a PDP-11. A clock gates the five scalar channels to accumulate pulses for 1 ms time intervals. At the end of each interval, the contents of the registers are transferred to the PDP-11 for temporary storage and the scalars are reset. After each shot the accumulated data is sent to the DEC-10 computer for permanent archiving. In between discharges, the analysis program accesses the raw data, time averages over a 10 ms interval, performs quality analysis of the data (e.g. signal-to-noise ratio), corrects for the background level due to noise counts, applies the energy dependent calibration calculations, and finally performs a least squares fit between user supplied energy limits to a semilog plot of the data points as a function of energy. Three basic displays are then available at the charge exchange system control console.

The display shown in Fig. 2 is automatically provided after each discharge. Shown on the left are the raw data signals from the five detector channels with the energy setting of each channel indicated in the upper left corner of the plot. The other frames are semilog energy distributions used to provide a rough ion temperature measurement at two user supplied time points for the current shot.

To obtain an ion temperature measurement for a given set of discharge conditions, it is usually necessary to accumulate data from 3-7 shots under reproducible conditions. The range of energies encompassed by the analyzer channels is varied

with each shot to provide a cumulated semilog display of data such as that shown in Fig. 3. The energy limits for the least squares line fit shown are selected by inspection of the built up data display. Such line fits, the slope of which yields the ion temperature, are provided for each 10 ms time interval throughout the discharge. The resulting display of ion temperature versus discharge time is shown in Fig. 4.

The position of the thermal charge exchange analyzer relative to the neutral beam injectors is indicated by the arrow in Fig. 5. The analyzer line-of-sight does not intersect the injection region of the adjacent beam lines.

The data base for neutral injection heating was obtained by varying the beam power ($P_B \sim 0.7 - 2.4$ MW), beam/plasma species combination (H, D), and initial plasma electron density ($\bar{n}_e(I) \sim 0.9 - 3.6 \times 10^{13} \text{ cm}^{-3}$), where $\bar{n}_e(I)$ is the line average electron density at the onset of injection. In general, the line average electron density increases during injection. The value at the time of peak ion temperature is designated either by $\bar{n}_e(P)$ or simply \bar{n}_e . For all data reported here, the high Z impurity content of the plasma was minimized by use of water-cooled carbon limiters and titanium gettering. The radius of the carbon limiters (located top and bottom of the plasma) was always $a = 40$ cm. Various combinations of co- and counter-injecting beams were used, but most injection experiments (and hence ion temperature results presented in this report) employed all four beam-lines (2 co- and 2 counter-injection).

Selection of the charge exchange ion temperature measurements presented in the report was performed in the following manner. A total of 526 discharges were selected from heating experiments over the reporting period (July 21 - October 13, 1978) for which the raw charge exchange data and beam performance appeared reliable. Each discharge was then examined to reject data for which one or more of the intended beam lines did not inject for the prescribed pulse

duration (i.e. faulted part way through the desired pulse period). This reduced the data base to 188 shots distributed over approximately 27 experimental runs. The charge exchange energy distributions for these runs were analyzed at 10 ms time steps to obtain the ion temperature as a function of discharge time. On the basis of the quality of the charge exchange data (e.g. reliable zero level, adequate number of discharges, etc.) the data base was further reduced to 118 discharges distributed over 21 heating experiments.

Examples of the charge exchange energy distribution and time evolution of the ion temperature are shown in Fig. 6-13. The top of each figure shows charge exchange energy distributions during the ion temperature rise corresponding to times indicated by the vertical arrows on the ion temperature versus discharge time evolution which appears at the bottom. Some salient parameters for each data display are noted on the figures. Further information is presented in Appendix I in the form of data files. Also contained in Appendix I are the data files for the remainder of the charge exchange data base. An explanation of the terminology used in these files is given on the cover page preceding this data compilation.

A collation containing most of the charge exchange ion temperature measurements is given in Fig. 14. This plot shows the peak ion temperature attained during heating experiments at various points in the beam power/plasma density parameter space. The electron density corresponds to the line average value at or after peak ion temperature was reached. To avoid excessive crowding in the plot, several data files were omitted. All of the ion temperature measurements presented above are uncorrected for plasma profile effects. The raw data usually is an underestimate of the actual ion temperature at the center of the plasma.³ This topic will be discussed further in the Section IV.

III. ANALYSIS OF THE CHARGE EXCHANGE MEASUREMENTS

The experimental scenario obviously invites determining the dependence of the ion temperature rise on injected beam power and plasma density. First,

the ratio of the ion temperature increase to beam power, $\Delta T_i/P_B$, is plotted as a function of electron density in Fig. 15. Although the data scatter does not permit a precise determination of the density dependence, it is reasonable to accept the scaling $\Delta T_i/P_B \propto 1/\bar{n}_e$. In Fig. 16, the ion temperature increase is plotted as a function of P_B/\bar{n}_e . A least squares fit to the data yields the empirical relationship:

$$\Delta T_i \text{ (keV)} = 4.5 \pm 0.5 \frac{P_B \text{ (MW)}}{\bar{n}_e (\times 10^{13} \text{ cm}^{-3})} \quad (1)$$

The solid line depicts this relation with the satellite lines (dashed) corresponding to the error limits on the slope. The peak ion temperature is plotted against P_B/\bar{n}_e in Fig. 17. Also shown is the pre-injection ion temperature associated with each data point. The solid data points represent runs in which the microwave diagnostic exhibited an abrupt density increase shortly after attainment of peak ion temperature. This event correlates with the onset of density fluctuations observed by microwave scattering diagnostics.⁴ It is tempting to ascribe this behavior to the onset of a new microinstability having a threshold at $T_i \approx 4$ keV. On the other hand, this threshold also corresponds to $P_B/\bar{n}_e \approx 0.8$, so the possibility of a direct beam induced instability cannot be excluded. In either case, the phenomenon is apparently innocuous from the heating viewpoint, since the ion temperature continues to rise following Eq. (1) despite the onset of the density fluctuations.

An attempt was made to determine the parametric dependence of the rise and fall times of the ion temperature. The rise/fall times quoted here correspond to the time interval between $0.10 \Delta T_i$ and $0.90 \Delta T_i$ determined from the $T_i(t)$ temporal plots. In Fig. 18, the rise/fall times are plotted as a function of $\langle \bar{n}_e \rangle = (\bar{n}_e(I) + \bar{n}_e(P))/2$. Again the data is insufficient to establish a definitive scaling. However, as can be seen the data is not inconsistent with a $1/\langle \bar{n}_e \rangle$ dependence. The rise/fall times multiplied by $\langle \bar{n}_e \rangle$ and plotted against

T_i in Fig. 19 show no clear T_i dependence. Further discussion of the charge exchange ion temperature rise/fall times is given in the next section.

IV. DISCUSSION

This section addresses an assortment of queries related to both the charge exchange measurements as well as aspects of the analysis given in the previous section.

First, the charge exchange energy distributions during beam injection exhibit a remarkably Maxwellian distribution. Traditionally, one expects an observable curvature in this region due to the radial variation of ion temperature (and neutral density), with the deduced ion temperature being a 10 - 20% underestimate of the central value. This was examined using a computer code which simulates the charge exchange distribution and corrects the apparent ion temperature to give the actual central value. The code divides the analyzer line-of-sight into 50 equal segments across the plasma diameter. Using $T_e(r)$ from electron cyclotron emission⁽⁵⁾ and Thomson scattering measurements along with $n_e(r)$ from the latter, and $n_0(r)$, $T_i(r)$ profiles estimated from the ion power balance computer code,⁽⁶⁾ the charge exchange production rate in each segment is calculated over a user specified range in 1 keV steps. Next, the attenuation of the charge exchange efflux from each segment at each energy due to charge exchange, and ionization due to ion, electron and impurity collisions is calculated for the appropriate path length out of the plasma. The resulting efflux is displayed as a function of energy along with the corrected central ion temperature value. A comparison with the measured energy distribution is made by normalizing the two distributions at a point within the experimental energy fitting limits and superimposing the spectra.

An example of this procedure is given using the charge exchange energy distribution corresponding to an apparent peak ion temperature of 3.6 keV in Fig. 6 (Data File: 2). This data was chosen because the relatively low temperature and typical density should exhibit the curvature effect in question. The

upper plot in Fig. 20 shows the neutral density radial profile generated from measured input plasma parameters by a simple neutral density calculation appropriate for large tokamaks⁽⁷⁾ that is coupled with the ion power balance code mentioned above, while the lower plot shows the input electron temperature profile and the resulting ion temperature profile generated by the ion power balance code. Using the code-supplied local plasma parameters, the charge exchange spectra is computed in the manner described above, yielding the result shown in the upper plot of Fig. 21. The solid line is fitted between the same energy limits (6 to 19 keV) as the measured spectrum shown in the bottom portion of the figure. In both cases, the slope of the lines yields a temperature of 3.6 keV. Although it is difficult to discern from the T_i profile shown in Fig. 21, the true central ion temperature returned by the code is 3.7 keV. In the lower plot of Fig. 21, the solid curve corresponds to the calculated spectrum which is normalized to the measured one at $E = 19$ keV.

From this display (and others not presented), the following statements can be made. First of all, the agreement between the two distributions demonstrates that the charge exchange measurements correspond to a bulk ion temperature which underestimates the central value by $\leq 5\%$. Second, the slight curvature evidenced by the calculated distribution is not discernable within the scatter of the experimental data. Furthermore, the peaked ion temperature profile whose gradient occurs over a region of modest variation in neutral density is responsible for the absence of significant curvature in the high energy regime of the experimental distributions. With increasing ion temperature, peaking of the T_i radial profile becomes more pronounced thereby further reducing this already small curvature.

Independently of the above profile effects, an important inaccuracy in the charge exchange ion temperature may arise if the thermal ion distribution is distorted by the presence of energetic beam ions in the plasma. A linearized

calculation of this effect for the quite different parameters of the CLEO tokamak injection experiments⁸ indicates substantial distortion when the calculation is extrapolated to PLT parameters.² Recent numerical work,^{9,10,11} however, based on the nonlinear Fokker-Planck equation,¹² predicts at most a small overestimate of the ion temperature (~ 5%) due to the slightly non-Maxwellian character of the thermal ion distribution, when the ion energy loss processes which balance the energy input from the neutral beams are assumed to be roughly independent of ion energy. On the other hand, if the loss process is taken to act only on low energy ions ($E_i \leq T_i$) as is implicitly assumed in the linearized calculation of Ref. 8, substantial distortions can be generated,⁹ giving as much as ~ 30% overestimate of the ion temperature measured by charge exchange. Since the dominant loss processes in the PLT case are believed to be charge exchange, electron-ion coupling and neoclassical ion thermal conduction — which are not strongly dependent on ion energy — the charge exchange measurements are expected to reflect the true central bulk ion temperature. This does not imply that the above effects might not occur to some degree. However, detection of these effects would impose stringent requirements on the quality of the charge exchange data, and other parameters as well. The charge exchange distribution, to begin with, ought to be determined well above and below the energy range of interest for ion temperature measurements ($E \sim 2 - 6 kT_i$), viewing both perpendicular and parallel to the toroidal field. Radial profiles of T_e , T_i , n_e and n_0 are desirable in order to unfold comparable distortions due to charge exchange generation/attenuation effects as discussed earlier. This implies accumulation of considerable data under tightly controlled experimental conditions. Unfortunately, the available data are not adequate to pursue these interesting effects.

Some aspects of the time evolution of the ion temperature with injection heating are considered next. Interpretation of the charge exchange ion

temperature rise and fall times is complicated by several competing effects having similar time scales. Some of the relevant characteristic times are discussed below.

The beam stopping time,¹³

$$\tau_{\text{stop}} = \frac{\tau_s}{3} \ln \left\{ \frac{v_o^3 + v_c^3}{v_i^3 + v_c^3} \right\} \quad (2)$$

characterizes the time required by the beam neutrals injected at an energy E_B to degrade into the thermal ion energy range, $3/2 kT_i$. In this equation

$$\tau_s = 6.32 \times 10^8 \frac{A_B T_e^{3/2} \text{ (eV)}}{n_e Z_B^2 \ln \Lambda_e} \quad (3)$$

is the Spitzer slowing-down time,¹⁴ where A_b , Z_b are the mass (in AMU) and charge, respectively, of the injected species and $\ln \Lambda_e \sim 13$ is the relativistic coulomb logarithm. This is the time required for the injected particle to e-fold in velocity solely due to drag on the electrons. In Eq. (2) the remaining terms are velocity parameters given by:

$$v_i = 1.384 \times 10^6 \left(\frac{1.5 T_i}{A_B} \right)^{1/2} \quad (4)$$

$$v_o = 1.384 \times 10^6 \left(E_B / A_B \right)^{1/2} \quad (5)$$

and

$$v_c = 5.33 \times 10^6 ([Z] / \bar{A}_i)^{1/2} T_e^{1/2} \quad (6)$$

where

$$\frac{[Z]}{\bar{A}_i} = \sum_i \frac{n_i}{n_e} \frac{Z_i^2 \ln \Lambda_i}{A_i \ln \Lambda_e} \quad (7)$$

Here n_i , Z_i , A_i are the density, charge state and mass of the hydrogenic and dominant impurity ion species. For the beam heating experiments the high Z content is low so that $[Z]/\bar{A}_i \sim 0.5 - 1.0$. Energies and temperatures are in eV units yielding velocity units of cm/sec.

The contribution of the stopping time to the measured ion temperature rise/fall times is obtained using the following input parameters in conjunction with Eq. (2):

$$T_e(0) = \frac{T_e(I) + T_e(P)}{2} \quad (8)$$

$$T_i(0) = \frac{T_i(I) + T_i(P)}{2} \quad (9)$$

$$n_e(0) = 2.2 \times \left\{ \frac{\bar{n}_e(I) + \bar{n}_e(P)}{2} \right\} \quad (10)$$

$$\bar{E}_B = 35 \text{ keV} \quad (11)$$

$$\frac{[Z]}{\bar{A}_i} = 0.75 \quad (12)$$

where \bar{E}_B is derived from the neutral beam injection records and the factor 2.2 in Eq. (10) is the average value for converting the line average electron density to the central value for these experiments. The notation I,P enclosed in parentheses designates the value at the onset of injection and at peak ion temperature, respectively. In Fig. 22, the calculated stopping time is compared with the ion temperature rise/fall times. A reasonable fit to the data is given by

$$\tau_r \text{ (ms)} = 25 + \tau_{\text{stop}} \quad (13)$$

and

$$\tau_f \text{ (ms)} = 50 + \tau_{\text{stop}} \quad (14)$$

where τ_r , τ_f are the measured rise and fall times, respectively. The results given by the above equations are relatively insensitive to variations of T_e , T_i about the mean value. The dependence on the beam energy, E_B , is significant, but the strongest dependence is on the value of the central electron density. Fortunately, the reliability of the measured electron density values is good.

In the framework of the simplified approach used here, comparison of the charge exchange ion temperature rise/fall times with characteristic beam/plasma time constants is useful only to attempt identification the dominant effects. With this caveat, the results shown in Fig. (22) provide a basis for some limited interpretation.

The variation of the measured rise/fall time with $1/\langle \bar{n}_e \rangle$ in Fig. 18 is explicable in terms of the density dependence of τ_{stop} . Furthermore, a large component of the measured times is attributable to the stopping time, the order of 50% or more. It is tempting to ascribe the difference between the measured times and τ_{stop} to the ion energy confinement time, τ_{Ei} . Ion power balance calculations yield $\tau_{Ei} = 25$ ms, this value being characteristic during the quasi-equilibrium interval around peak ion temperature under all neutral beam heating conditions presented in this report. This designation, however, is problematic in view of the difference between the rise and fall times. The observation that the fall times are consistently longer than the rise times by the order of 25 ms (or, conversely, the rise times are shorter by this amount) remains to be explained. Effects not accounted for in the present treatment which conceivably influence the rise/fall asymmetry, include: 1) time dependence of the magnitude of T_e and n_e which often exhibit temporal asymmetry experimentally;

Here n_i , Z_i , A_i are the density, charge state and mass of the hydrogenic and dominant impurity ion species. For the beam heating experiments the high Z content is low so that $[Z]/\bar{A}_i \sim 0.5 - 1.0$. Energies and temperatures are in eV units yielding velocity units of cm/sec.

The contribution of the stopping time to the measured ion temperature rise/fall times is obtained using the following input parameters in conjunction with Eq. (2):

$$T_e(0) = \frac{T_e(I) + T_e(P)}{2} \quad (8)$$

$$T_i(0) = \frac{T_i(I) + T_i(P)}{2} \quad (9)$$

$$n_e(0) = 2.2 \times \left\{ \frac{\bar{n}_e(I) + \bar{n}_e(P)}{2} \right\} \quad (10)$$

$$\bar{E}_B = 35 \text{ keV} \quad (11)$$

$$\frac{[Z]}{\bar{A}_i} = 0.75 \quad (12)$$

where \bar{E}_B is derived from the neutral beam injection records and the factor 2.2 in Eq. (10) is the average value for converting the line average electron density to the central value for these experiments. The notation I,P enclosed in parentheses designates the value at the onset of injection and at peak ion temperature, respectively. In Fig. 22, the calculated stopping time is compared with the ion temperature rise/fall times. A reasonable fit to the data is given by

$$\tau_r \text{ (ms)} = 25 + \tau_{\text{stop}} \quad (13)$$

and

$$\tau_f \text{ (ms)} = 50 + \tau_{\text{stop}} \quad (14)$$

where τ_r , τ_f are the measured rise and fall times, respectively. The results given by the above equations are relatively insensitive to variations of T_e , T_i about the mean value. The dependence on the beam energy, E_b , is significant, but the strongest dependence is on the value of the central electron density. Fortunately, the reliability of the measured electron density values is good.

In the framework of the simplified approach used here, comparison of the charge exchange ion temperature rise/fall times with characteristic beam/plasma time constants is useful only to attempt identification the dominant effects. With this caveat, the results shown in Fig. (22) provide a basis for some limited interpretation.

The variation of the measured rise/fall time with $1/\langle \bar{n}_e \rangle$ in Fig. 18 is explicable in terms of the density dependence of τ_{stop} . Furthermore, a large component of the measured times is attributable to the stopping time, the order of 50% or more. It is tempting to ascribe the difference between the measured times and τ_{stop} to the ion energy confinement time, τ_{Ei} . Ion power balance calculations yield $\tau_{Ei} = 25$ ms, this value being characteristic during the quasi-equilibrium interval around peak ion temperature under all neutral beam heating conditions presented in this report. This designation, however, is problematic in view of the difference between the rise and fall times. The observation that the fall times are consistently longer than the rise times by the order of 25 ms (or, conversely, the rise times are shorter by this amount) remains to be explained. Effects not accounted for in the present treatment which conceivably influence the rise/fall asymmetry include: 1) time dependence of the magnitude of T_e and n_e which often exhibit temporal asymmetry experimentally;

2) time dependence of the radial profiles known to occur from measurements for T_e , n_e and inferred from ion power balance considerations for T_i ; 3) the presence of an enhanced neutral density (and thus charge exchange loss) during the rise phase due to both injected neutrals and neutral gas influx from the heating beams; 4) droop in the beam power delivered to the plasma expected from experiments on reionization losses in the beam duct;^{15,16} and 5) enhanced transport due to density fluctuations which are observed for ion temperatures in excess of $T_i \sim 4$ keV. The last effect seems unlikely, since the asymmetry is also observed for $T_i < 4$ keV cases. At the present time, however, our simple analysis cannot decide between the possible causes. Further study of the rise/fall time phenomena using time-dependent computer codes is in progress. Upon completion of this work, it may be possible to make definitive statements on the temporal characteristics of the charge exchange ion temperature excursion due to neutral injection heating.

V. SUMMARY

The thermal charge exchange diagnostic measured central ion temperatures up to 6.6 keV for 2.4 MW-level neutral injection heating in low density PLT discharges. Throughout the heating experiments reported here, PLT was operated with 40 cm radius water-cooled carbon limiters and titanium gettering. Over the beam power ($P_B \sim 0.7 - 2.4$ MW) and plasma electron density ($\bar{n}_e \sim 1.6 - 3.6 \times 10^{13} \text{ cm}^{-3}$) parameters space thus far investigated, the ion temperature excursion, ΔT_i , is observed to scale as

$$\Delta T_i (\text{keV}) = 4.5 \pm 0.5 P_B (\text{MW}) / \bar{n}_e (\times 10^{13} \text{ cm}^{-3})$$

where \bar{n}_e is the line average electron density at peak ion temperature.

On the basis of a simple analysis, it is inferred that the beam stopping time accounts for more than half of the charge exchange ion temperature rise/fall

times as well as the observed $1/\langle \bar{n}_e \rangle$ scaling. The remaining portion of the rise/fall times, particularly the experimentally observed asymmetry between the two, remains to be explained.

ACKNOWLEDGMENTS

The authors appreciate the assistance and advice of H. P. Eubank and R. J. Goldston in various aspects of the charge exchange ion temperature diagnostics. We thank L. R. Grisham for providing a careful compilation of the injected beam power as well as P. C. Efthimion and the Thomson scattering group for providing the electron temperature measurements included in this report. This work was supported by the United States Department of Energy Contract No. EY-76-C-02-3073.

REFERENCES

1. S. L. Davis, S. S. Medley and M. Brusati, "The Charge Exchange Analyzer for Mass Resolved Ion Temperature Measurements on PLT," PPL-1478 (1978).
2. H. P. Eubank, et al., "PLT Neutral Beam Heating Results," IAEA-CN-37-C-3, Innsbruck, Austria (1978), also PPL-1491.
3. C. R. Parsons and S. S. Medley, "On the Interpretation of Charge-Exchange Ion Temperature Measurements in Tokamaks," Plasma Phys. 16, 267 (1974).
4. V. Arunasalam, P. Efthimion, B. Gaulke, J. Hosea, E. Mazzucato, and M. Yamada, "Enhanced Level of Low-Frequency Microturbulence in PLT During Neutral Beam Heating," Bull. Am. Phys. Soc., Vol. 23, Nov. 7, p. 901, 1978.
5. P. C. Efthimion, V. Arunasalam, and J. C. Hosea, Bull. of Am. Phys. Soc., 23, 901 (1978).
6. S. L. Davis, et al., "Ion Power Balance in PLT During Neutral Injection," in preparation.
7. R. J. Goldston, "A Simple Neutral Density Profile Calculation for Tokamaks with $\lambda_{mfp} \ll a$," PPL-1443 (1978). To be published in Plasma Physics.
8. J. G. Cordey, in Plasma Physics and Controlled Nuclear Fusion Research (Proceedings of the 5th International Conference, Tokyo, Japan, 1974) Vol. 1, IAEA, Vienna, Austria (1975) 623.
9. R. Kulsrud and Y. Sun, private communication, (PPPL).
10. R. J. Goldston, private communication, (PPPL).
11. A. Mirin, private communication, (LLL).
12. J. Killeen and K. D. Marx, Methods of Computational Physics, 9, B. Alder, editor; Academic Press, New York (1970) 422.
13. R. J. Goldston, "Fast Ion Diagnostic Experiment on ATC: Radially Resolved Measurements of q , Z_{eff} , $T_{i||}$ and $T_{i\perp}$," Ph.D. Thesis, Princeton University (1975). Unpublished.

14. L. Spitzer, Jr., Physics of Fully Ionized Gases, Interscience, Second Edition (1967) p. 135.
15. L. D. Stewart, "Neutral Beam System Reionization Losses," PPL-1469 (1978).
16. L. R. Grisham, et al., "PLT Neutral Injector Performance," PPL-1484 (1978).

APPENDIX I.

DATA FILES FOR CHARGE EXCHANGE
ION TEMPERATURE MEASUREMENTS

This table is a chronological compilation of the charge exchange measurements and related parameters presented in this report. Most of the terminology used in the data files is self-explanatory. Further explanation of a few of the terms is given below.

ΔT_i \equiv Peak central ion temperature minus pre-injection ion temperature.

Δt \equiv Rise/fall times for temperature excursion between 0.1 ΔT_i and 0.9 ΔT_i .

INJECTORS \equiv Co-injectors are designated East and West; counter-injectors, North and South.

$\bar{n}_e(I)$ \equiv Pre-injection line average electron density.

$\bar{n}_e(P)$ \equiv Line average electron density at/or just following attainment of peak ion temperature.

$T_e(I), T_e(P)$ \equiv Central electron temperature at time corresponding to start of injection, $T_e(I)$, and peak electron temperature, $T_e(P)$. Values shown are intended to be only indicative of the core region of the discharge with radial and temporal details roughly averaged - use with caution.

DATA FILE: 1

| | | |
|----------------|---|----------------------------|
| <u>ARCHIVE</u> | DATE: July 20, 1978 | SHOT NUMBERS: <u>34158</u> |
| | | <u>60</u> |
| | SCENARIO: H ⁰ + D ⁺ | <u>63</u> |
| | | <u>66</u> |
| | CX. LOG: JY20S | <u>73</u> |
| | | <u> </u> |
| | | <u> </u> |

ION TEMPERATURE MEASUREMENTS

PEAK $T_i(r=0)$: 2.7 keV
 $\Delta T_i(r=0)$: 2.1 keV
 $\Delta t(\text{rise})$: - ms
 $\Delta t(\text{fall})$: - ms

BEAM PARAMETERS

| | |
|-----------------------------|----------------------|
| INJECTORS: 1CO(E) + 1CTR(S) | CO POWER: 0.30 MW |
| DURATION: 100 ms | CTR POWER: 0.39 MW |
| START: 450 ms | TOTAL POWER: 0.69 MW |

PLASMA PARAMETERS

| | |
|---|------------------|
| $\bar{n}_e(I)$: $1.2 \times 10^{13} \text{ cm}^{-3}$ | $T_e(I)$: - keV |
| $\bar{n}_e(P)$: $2.0 \times 10^{13} \text{ cm}^{-3}$ | $T_e(P)$: - keV |

REMARKS: NO DENSITY FLUCTUATIONS.

DATA FILE: 2

| | | |
|----------------|---|----------------------------|
| <u>ARCHIVE</u> | DATE: July 21, 1978 | SHOT NUMBERS: <u>34275</u> |
| | | <u>76</u> |
| | SCENARIO: H ⁰ + D ⁺ | <u>77</u> |
| | | <u>83</u> |
| | CX. LOG: JY21Q | <u>90</u> |
| | | <u>93</u> |
| | | <u> </u> |

ION TEMPERATURE MEASUREMENTS

PEAK $T_i(r=0)$: 3.6 keV
 $\Delta T_i(r=0)$: 2.7 keV
 $\Delta t(\text{rise})$: 65 ms
 $\Delta t(\text{fall})$: 103 ms

BEAM PARAMETERS

| | |
|------------------|----------------------|
| INJECTORS: 4 | CO POWER: 0.80 MW |
| DURATION: 100 ms | CTR POWER: 0.60 MW |
| START: 450 ms | TOTAL POWER: 1.40 MW |

PLASMA PARAMETERS

| | |
|---|--------------------|
| $\bar{n}_e(I)$: $1.1 \times 10^{13} \text{ cm}^{-3}$ | $T_e(I)$: 2.8 keV |
| $\bar{n}_e(P)$: $2.2 \times 10^{13} \text{ cm}^{-3}$ | $T_e(P)$: 3.3 keV |

REMARKS: NO DENSITY FLUCTUATIONS.
 SEE FIG. 6 FOR DATA PLOT.

DATA FILE: 3

| | | | |
|----------------|---|---------------|-------|
| <u>ARCHIVE</u> | DATE: July 21, 1978 | SHOT NUMBERS: | 34242 |
| | | | 45 |
| | SCENARIO: H ^o → D ⁺ | | 46 |
| | | | 51 |
| | CX. LOG: JY21S | | 53 |
| | | | |
| | | | |

ION TEMPERATURE MEASUREMENTS

PEAK $T_i(r=0)$: 2.8 keV
 $\Delta T_i(r=0)$: 2.0 keV
 $\Delta t(\text{rise})$: 67 ms
 $\Delta t(\text{fall})$: 100 ms

BEAM PARAMETERS

| | | | |
|------------|---------------|--------------|---------|
| INJECTORS: | 1CO(E) + 2CTR | CO POWER: | 0.50 MW |
| DURATION: | 100 ms | CTR POWER: | 0.62 MW |
| START: | 450 ms | TOTAL POWER: | 1.12 MW |

PLASMA PARAMETERS

| | | | |
|------------------|--------------------------------------|------------|---------|
| $\bar{n}_e(I)$: | $1.0 \times 10^{13} \text{ cm}^{-3}$ | $T_e(I)$: | 2.2 keV |
| $\bar{n}_e(P)$: | $2.0 \times 10^{13} \text{ cm}^{-3}$ | $T_e(P)$: | 2.8 keV |

REMARKS: NO DENSITY FLUCTUATIONS.
SEE FIG. 7 FOR DATA PLOT.

DATA FILE: 4ARCHIVE

DATE: July 21, 1978

SHOT NUMBERS: 34275SCENARIO: $H^{\circ} \rightarrow D^{\dagger}$ 76809099

CX. LOG: JY21'

ION TEMPERATURE
MEASUREMENTSPEAK $T_i(r=0)$: 3.9 keV $\Delta T_i(r=0)$: 3.2 keV $\Delta t(\text{rise})$: 53 ms $\Delta t(\text{fall})$: 85 msBEAM PARAMETERS

INJECTORS: 4

CO POWER: 0.87 MW

DURATION: 100 ms

CTR POWER: 0.67 MW

START: 450 ms

TOTAL POWER: 1.54 MW

PLASMA PARAMETERS $\bar{n}_e(I)$: $1.1 \times 10^{13} \text{ cm}^{-3}$ $T_e(I)$: 2.8 keV $\bar{n}_e(P)$: $2.3 \times 10^{13} \text{ cm}^{-3}$ $T_e(P)$: 3.2 keVREMARKS: NO DENSITY FLUCTUATIONS.

DATA FILE: 5

| | | | |
|----------------|---|---------------|---------------|
| <u>ARCHIVE</u> | DATE: July 25, 1978 | SHOT NUMBERS: | <u>65126</u> |
| | | | <u>28</u> |
| | SCENARIO: D ^o → H ⁺ | | <u>29</u> |
| | | | <u>31</u> |
| | CX. LOG: JY25S | | <u> </u> |
| | | | <u> </u> |
| | | | <u> </u> |

ION TEMPERATURE MEASUREMENTS

PEAK $T_i(r=0)$: 5.0 keV
 $\Delta T_i(r=0)$: 4.0 keV
 $\Delta t(\text{rise})$: 77 ms
 $\Delta t(\text{fall})$: 77 ms

BEAM PARAMETERS

| | |
|------------------|----------------------|
| INJECTORS: 4 | CO POWER: 1.15 MW |
| DURATION: 100 ms | CTR POWER: 0.58 MW |
| START: 450 ms | TOTAL POWER: 1.73 MW |

PLASMA PARAMETERS

| | |
|---|--------------------|
| $\bar{n}_e(I)$: $1.4 \times 10^{13} \text{ cm}^{-3}$ | $T_e(I)$: 1.6 keV |
| $\bar{n}_e(P)$: $1.8 \times 10^{13} \text{ cm}^{-3}$ | $T_e(P)$: 2.8 keV |

REMARKS: DENSITY FLUCTUATION ONSET AT ~ 520 ms.

DATA FILE: 6ARCHIVE

DATE: July 23, 1978

SHOT NUMBERS: 8755962SCENARIO: $D^{\circ} \rightarrow H^{+}$ 6465

CX. LIB: JY28S

ION TEMPERATURE
MEASUREMENTSPEAK $T_i(r=0)$: 3.6 keV $\Delta T_i(r=0)$: 2.9 keV $\Delta t(\text{rise})$: - ms $\Delta t(\text{fall})$: - msBEAM PARAMETERS

INJECTORS: 4

CO POWER: 1.23 MW

DURATION: 150 ms

CTR POWER: 0.74 MW

START: 400 ms

TOTAL POWER: 1.97 MW

PLASMA PARAMETERS $\bar{n}_e(I)$: $3.6 \times 10^{13} \text{ cm}^{-3}$ $T_e(I)$: 0.9 keV $\bar{n}_e(P)$: $3.6 \times 10^{13} \text{ cm}^{-3}$ $T_e(P)$: 2.0 keVREMARKS: NO DENSITY FLUCTUATIONS.

DATA FILE: 7

| | | | |
|----------------|---|---------------|-------|
| <u>ARCHIVE</u> | DATE: August 3, 1978 | SHOT NUMBERS: | 88399 |
| | | | 400 |
| | SCENARIO: D ^o → H ⁺ | | 402 |
| | | | 417 |
| | CX. LOG: AU03S | | 425 |
| | | | 431 |

ION TEMPERATURE MEASUREMENTS

PEAK $T_i(r=0)$: 5.9 keV
 $\Delta T_i(r=0)$: 5.1 keV
 $\Delta t(\text{rise})$: 38 ms
 $\Delta t(\text{fall})$: 62 ms

BEAM PARAMETERS

| | |
|------------------|----------------------|
| INJECTORS: 4 | CO POWER: 1.15 MW |
| DURATION: 150 ms | CTR POWER: 0.90 MW |
| START: 450 ms | TOTAL POWER: 2.05 MW |

PLASMA PARAMETERS

| | |
|---|--------------------|
| $\bar{n}_e(I)$: $0.9 \times 10^{13} \text{ cm}^{-3}$ | $T_e(I)$: 2.4 keV |
| $\bar{n}_e(P)$: $1.9 \times 10^{13} \text{ cm}^{-3}$ | $T_e(P)$: 2.9 keV |

REMARKS: DENSITY FLUCTUATION ONSET AT ~ 550 ms.
 SEE FIG. 8 FOR DATA PLOT.

DATA FILE: 8

| | | |
|---|----------------------|---------------------|
| <u>ARCHIVE</u> | DATE: August 3, 1978 | SHOT NUMBERS: 88419 |
| | | 20 |
| SCENARIO: D ^o → H ⁺ | | 31 |
| | | 35 |
| CX. LOG: AU03Z | | 40 |
| | | 41 |
| | | |

ION TEMPERATURE MEASUREMENTS

PEAK $T_i(r=0)$: 6.0 keV
 $\Delta T_i(r=0)$: 5.0 keV
 $\Delta t(\text{rise})$: 68 ms
 $\Delta t(\text{fall})$: 107 ms

BEAM PARAMETERS

| | |
|------------------|----------------------|
| INJECTORS: 4 | CO POWER: 1.10 MW |
| DURATION: 150 ms | CTR POWER: 0.90 MW |
| START: 450 ms | TOTAL POWER: 2.00 MW |

PLASMA PARAMETERS

| | |
|---|--------------------|
| $\bar{n}_e(I)$: $1.0 \times 10^{13} \text{ cm}^{-3}$ | $T_e(I)$: 2.4 keV |
| $\bar{n}_e(P)$: $1.9 \times 10^{13} \text{ cm}^{-3}$ | $T_e(P)$: 3.0 keV |

REMARKS: DENSITY FLUCTUATION ONSET AT ~ 550 ms.

| | | |
|----------------|---|----------------------------|
| <u>ARCHIVE</u> | DATE: August 15, 1978 | SHOT NUMBERS: <u>88831</u> |
| | | <u>32</u> |
| | SCENARIO: H ⁰ → D ⁺ | <u>33</u> |
| | | <u>34</u> |
| | CX. LOG: AU15S | <u>35</u> |
| | | <u>39</u> |
| | | <u>40</u> |

ION TEMPERATURE MEASUREMENTS

PEAK $T_i(r=0)$: 3.6 keV
 $\Delta T_i(r=0)$: 2.8 keV
 $\Delta t(\text{rise})$: 53 ms
 $\Delta t(\text{fall})$: 77 ms

BEAM PARAMETERS

| | |
|------------------|----------------------|
| INJECTORS: 4 | CO POWER: 0.90 MW |
| DURATION: 150 ms | CTR POWER: 0.88 MW |
| START: 450 ms | TOTAL POWER: 1.78 MW |

PLASMA PARAMETERS

| | |
|---|--------------------|
| $\bar{n}_e(I)$: $1.6 \times 10^{13} \text{ cm}^{-3}$ | $T_e(I)$: 1.7 keV |
| $\bar{n}_e(P)$: $2.8 \times 10^{13} \text{ cm}^{-3}$ | $T_e(P)$: 2.7 keV |

REMARKS: NO DENSITY FLUCTUATIONS.
 SEE FIG. 9 FOR DATA PLOT.

A10

DATA FILE: 10

ARCHIVE

DATE: August 18, 1978

SHOT NUMBERS: 89067

68

SCENARIO: $D^0 + H^+$

69

71

CX. LOG: Au18S

ION TEMPERATURE
MEASUREMENTS

PEAK $T_i(r=0)$: 4.5 keV

$\Delta T_i(r=0)$: 3.7 keV

$\Delta t(\text{rise})$: - ms

$\Delta t(\text{fall})$: - ms

BEAM PARAMETERS

INJECTORS: 4

CO POWER: 1.23 MW

DURATION: 150 ms

CTR POWER: 1.10 MW

START: 400 ms

TOTAL POWER: 2.33 MW

PLASMA PARAMETERS

$\bar{n}_e(I)$: $1.4 \times 10^{13} \text{ cm}^{-3}$

$T_e(I)$: 2.0 keV

$\bar{n}_e(P)$: $2.6 \times 10^{13} \text{ cm}^{-3}$

$T_e(P)$: 2.5 keV

REMARKS: DENSITY FLUCTUATION ONSET AT ~ 500 ms.

DATA FILE: 11

| | | |
|----------------|---|---------------------|
| <u>ARCHIVE</u> | DATE: August 18, 1978 | SHOT NUMBERS: 89086 |
| | | 87 |
| | SCENARIO: D ^o → H ⁺ | 88 |
| | | |
| | CX. LOG: AU18U | |
| | | |
| | | |

ION TEMPERATURE MEASUREMENTS

PEAK $T_i(r=0)$: 6.6 keV
 $\Delta T_i(r=0)$: 5.5 keV
 $\Delta t(\text{rise})$: 70 ms
 $\Delta t(\text{fall})$: 104 ms

BEAM PARAMETERS

| | |
|------------------|----------------------|
| INJECTORS: 4 | CO POWER: 1.26 MW |
| DURATION: 150 ms | CTR POWER: 1.05 MW |
| START: 450 ms | TOTAL POWER: 2.31 MW |

PLASMA PARAMETERS

| | |
|---|--------------------|
| $\bar{n}_e(I)$: $1.4 \times 10^{13} \text{ cm}^{-3}$ | $T_e(I)$: 2.6 keV |
| $\bar{n}_e(P)$: $1.9 \times 10^{13} \text{ cm}^{-3}$ | $T_e(P)$: 3.8 keV |

REMARKS: DENSITY FLUCTUATION ONSET AT ~ 500 ms.
SEE FIG. 10 FOR DATA PLOT.

A12

DATA FILE: 12

ARCHIVE

DATE: August 18, 1978

SHOT NUMBERS: 89091

96

SCENARIO: D° → H°

101

103

CX. LOG: AU18W

104

ION TEMPERATURE
MEASUREMENTS

PEAK $T_i(r=0)$: 6.0 keV

$\Delta T_i(r=0)$: 5.0 keV

$\Delta t(\text{rise})$: - ms

$\Delta t(\text{fall})$: - ms

BEAM PARAMETERS

INJECTORS: 4

CO POWER: 1.23 MW

DURATION: 150 ms

CTR POWER: 0.94 MW

START: 450 ms

TOTAL POWER: 2.14 MW

PLASMA PARAMETERS

$\bar{n}_e(I)$: $1.0 \times 10^{13} \text{ cm}^{-3}$

$T_e(I)$: 3.0 keV

$\bar{n}_e(P)$: $2.0 \times 10^{13} \text{ cm}^{-3}$

$T_e(P)$: 4.0 keV

REMARKS: DENSITY FLUCTUATION ONSET AT ~ 570 ms.

DATA FILE: 13

| | | | |
|----------------|---|---------------|--------------|
| <u>ARCHIVE</u> | DATE: AUGUST 22, 1978 | SHOT NUMBERS: | <u>89320</u> |
| | | | <u>21</u> |
| | SCENARIO: D ⁰ → H ⁺ | | <u>22</u> |
| | | | <u>23</u> |
| | CX. LOG: AU22S | | <u>-----</u> |
| | | | <u>-----</u> |
| | | | <u>-----</u> |

ION TEMPERATURE MEASUREMENTS

PEAK $T_i(r=0)$: 5.0 keV
 $\Delta T_i(r=0)$: 4.0 keV
 $\Delta t(\text{rise})$: - ms
 $\Delta t(\text{fall})$: - ms

BEAM PARAMETERS

| | |
|------------------|----------------------|
| INJECTORS: 4 | CO POWER: 1.36 MW |
| DURATION: 150 ms | CTR POWER: 1.02 MW |
| START: 450 ms | TOTAL POWER: 2.38 MW |

PLASMA PARAMETERS

| | |
|---|------------------|
| $\bar{n}_e(I)$: $1.4 \times 10^{13} \text{ cm}^{-3}$ | $T_e(I)$: - keV |
| $\bar{n}_e(P)$: $2.7 \times 10^{13} \text{ cm}^{-3}$ | $T_e(P)$: - keV |

REMARKS: DENSITY FLUCTUATION ONSET AT ~ 530 ms.

| | | |
|----------------|---|---------------------|
| <u>ARCHIVE</u> | DATE: August 23, 1978 | SHOT NUMBERS: 89478 |
| | | 79 |
| | SCENARIO: D ^o + H ⁺ | 82 |
| | | 83 |
| | CX. LOG: AU23S | |
| | | |
| | | |
| | | |

ION TEMPERATURE MEASUREMENTS

PEAK $T_i(r=0)$: 4.0 keV
 $\Delta T_i(r=0)$: 3.5 keV
 $\Delta t(\text{rise})$: 54 ms
 $\Delta t(\text{fall})$: - ms

BEAM PARAMETERS

| | |
|--------------------------|----------------------|
| INJECTORS: 2CO + 1CTR(S) | CO POWER: 1.28 MW |
| DURATION: 150 ms | CTR POWER: 0.53 MW |
| START: 400 ms | TOTAL POWER: 1.81 MW |

PLASMA PARAMETERS

| | |
|---|--------------------|
| $\bar{n}_e(I)$: $1.5 \times 10^{13} \text{ cm}^{-3}$ | $T_e(I)$: 0.7 keV |
| $\bar{n}_e(P)$: $3.0 \times 10^{13} \text{ cm}^{-3}$ | $T_e(P)$: 2.7 keV |

REMARKS: NO DENSITY FLUCTUATIONS.
 SEE FIG. 12 FOR DATA PLOT.

DATA FILE: 16

| | | | |
|----------------|---|---------------|-------------------|
| <u>ARCHIVE</u> | DATE: August 23, 1978 | SHOT NUMBERS: | <u>89489</u> |
| | | | <u>90</u> |
| | SCENARIO: D ⁰ + H ⁺ | | <u>94</u> |
| | | | <u>98</u> |
| | CX. LOG: AU23U | | <u> </u> |
| | | | <u> </u> |
| | | | <u> </u> |

ION TEMPERATURE MEASUREMENTS

PEAK $T_i(r=0)$: 3.3 keV
 $\Delta T_i(r=0)$: 2.8 keV
 $\Delta t(\text{rise})$: - ms
 $\Delta t(\text{fall})$: - ms

BEAM PARAMETERS

| | |
|-----------------------------|----------------------|
| INJECTORS: 1CO(W) + 1CTR(S) | CO POWER: 0.54 MW |
| DURATION: 150 ms | CTR POWER: 0.53 MW |
| START: 400 ms | TOTAL POWER: 1.07 MW |

PLASMA PARAMETERS

| | |
|---|------------------|
| $\bar{n}_e(I)$: $1.6 \times 10^{13} \text{ cm}^{-3}$ | $T_e(I)$: - keV |
| $\bar{n}_e(P)$: $1.6 \times 10^{13} \text{ cm}^{-3}$ | $T_e(P)$: - keV |

REMARKS: NO DENSITY FLUCTUATIONS.

| | | |
|----------------|---|----------------------------|
| <u>ARCHIVE</u> | DATE: August 24, 1978 | SHOT NUMBERS: <u>89561</u> |
| | | <u>62</u> |
| | SCENARIO: D ^o → H ⁺ | <u>64</u> |
| | | <u>65</u> |
| | CX. LOG: AU24S | <u>66</u> |
| | | <u> </u> |
| | | <u> </u> |

ION TEMPERATURE MEASUREMENTS

PEAK $T_i(r=0)$: 4.6 keV
 $\Delta T_i(r=0)$: 3.9 keV
 $\Delta t(\text{rise})$: - ms
 $\Delta t(\text{fall})$: - ms

BEAM PARAMETERS

| | |
|------------------|----------------------|
| INJECTORS: 4 | CO POWER: 1.41 MW |
| DURATION: 150 ms | CTR POWER: 0.80 MW |
| START: 400 ms | TOTAL POWER: 2.21 MW |

PLASMA PARAMETERS

| | |
|---|------------------|
| $\bar{n}_e(I)$: $1.4 \times 10^{13} \text{ cm}^{-3}$ | $T_e(I)$: - keV |
| $\bar{n}_e(P)$: $2.7 \times 10^{13} \text{ cm}^{-3}$ | $T_e(P)$: - keV |

REMARKS: DENSITY FLUCTUATION ONSET AT ~ 540 ms.

DATA FILE: 20

| | | |
|-------------------------------|------------------------|----------------------------|
| <u>ARCHIVE</u> | DATE: October 12, 1978 | SHOT NUMBERS: <u>94938</u> |
| | | <u>39</u> |
| SCENARIO: D° → H ⁺ | | <u>40</u> |
| | | <u>48</u> |
| CX. LOG: OC12C | | <u>53</u> |
| | | <u>56</u> |
| | | <u> </u> |

ION TEMPERATURE MEASUREMENTS

PEAK $T_i(r=0)$: 1.7 keV
 $\Delta T_i(r=0)$: 0.9 keV
 $\Delta t(\text{rise})$: 37 ms
 $\Delta t(\text{fall})$: 65 ms

BEAM PARAMETERS

| | |
|-----------------------------|----------------------|
| INJECTORS: 1CO(W) + 1CTR(S) | CO POWER: 0.62 MW |
| DURATION: 150 ms | CTR POWER: 0.58 MW |
| START: 450 ms | TOTAL POWER: 1.20 MW |

PLASMA PARAMETERS

| | |
|---|--------------------|
| $\bar{n}_e(I)$: $3.0 \times 10^{13} \text{ cm}^{-3}$ | $T_e(I)$: 1.2 keV |
| $\bar{n}_e(P)$: $3.0 \times 10^{13} \text{ cm}^{-3}$ | $T_e(P)$: 1.8 keV |

REMARKS: NO DENSITY FLUCTUATIONS.

| | | |
|----------------|---|----------------------------|
| <u>ARCHIVE</u> | DATE: October 13, 1978 | SHOT NUMBERS: <u>94987</u> |
| | | <u>88</u> |
| | SCENARIO: D ^o → H ⁺ | <u>94</u> |
| | | <u>99</u> |
| | CX. LOG: OC135 | <u>95001</u> |
| | | <u>28</u> |
| | | <u> </u> |

ION TEMPERATURE MEASUREMENTS

PEAK $T_i(r=0)$: 2.6 keV
 $\Delta T_i(r=0)$: 2.0 keV
 $\Delta t(\text{rise})$: 50 ms
 $\Delta t(\text{fall})$: 68 ms

BEAM PARAMETERS

| | |
|------------------|----------------------|
| INJECTORS: 2C0 | CO POWER: 1.35 MW |
| DURATION: 150 ms | CTR POWER: — MW |
| START: 450 ms | TOTAL POWER: 1.35 MW |

PLASMA PARAMETERS

| | |
|---|--------------------|
| $\bar{n}_e(I)$: $3.0 \times 10^{13} \text{ cm}^{-3}$ | $T_e(I)$: 1.0 keV |
| $\bar{n}_e(P)$: $3.0 \times 10^{13} \text{ cm}^{-3}$ | $T_e(P)$: 1.6 keV |

REMARKS: NO DENSITY FLUCTUATIONS.
 SEE FIG. 13 FOR DATA PLOT.

FIGURE CAPTIONS

- Figure 1. Photograph of the 5-channel, mass-resolved charge-exchange analyzer used for PLT ion temperature measurements. (PPL-786347)
- A. Stripping cell.
 - B. He gas inlet.
 - C. Ion gauge access.
 - D. Turbo-pump port.
 - E. Magnet (provides energy analysis).
 - F. Electrostatic plates (provides mass analysis).
 - G. Channel electron multiplier detectors.
 - H. Signal Interface.
- Figure 2. Computer generated display of the charge exchange system raw signals. (PPL-786073)
- Figure 3. Semilog display of the charge exchange energy distribution. The factor f corresponds to $E^{-1/2} dN/dE$ where dN/dE is the charge exchange efflux after unfolding the calibrated energy dependent analyzer sensitivity. The abscissa scale is number of e-foldings. (PPL-783883)
- Figure 4. Typical display of ion temperature as a function of discharge time provided by the charge exchange diagnostic. (PPL-783872)
- Figure 5. Location of the charge exchange diagnostic on PLT relative to the neutral beam injectors. (PPL-783851)
- Figure 6. Charge exchange data for 1.5 MW neutral hydrogen injection into $\bar{n}_e(I) = 1.1 \times 10^{13} \text{ cm}^{-3}$ deuterium plasma. See Data File: 2. (PPL-786356)
- Figure 7. Charge exchange data for 1.1 MW neutral hydrogen injection into $\bar{n}_e(I) = 1.0 \times 10^{13} \text{ cm}^{-3}$ deuterium plasma. See Data File: 3. (PPL-786351)
- Figure 8. Charge exchange data for 2.1 MW neutral deuterium injection into $\bar{n}_e(I) = 0.9 \times 10^{13} \text{ cm}^{-3}$ hydrogen plasma. See Data File: 7. (PPL-786354)
- Figure 9. Charge exchange data for 1.8 MW neutral hydrogen injection into $\bar{n}_e(I) = 1.6 \times 10^{13} \text{ cm}^{-3}$ hydrogen plasma. See Data File: 9. (PPL-786353)

- Figure 10. Charge exchange data for 2.3 MW neutral deuterium injection into $\bar{n}_e(I) = 1.4 \times 10^{13} \text{ cm}^{-3}$ hydrogen plasma. See Data File: 11. (PPL-786357)
- Figure 11. Charge exchange data for 2.4 MW neutral deuterium injection into $\bar{n}_e(I) = 1.5 \times 10^{13} \text{ cm}^{-3}$ hydrogen plasma. See Data File: 14. (PPL-786352)
- Figure 12. Charge exchange data for 1.8 MW neutral deuterium injection into $\bar{n}_e(I) = 1.5 \times 10^{13} \text{ cm}^{-3}$ hydrogen plasma. See Data File: 15. (PPL-786355)
- Figure 13. Charge exchange data for 1.35 MW neutral deuterium injection into $\bar{n}_e(I) = 3.0 \times 10^{13} \text{ cm}^{-3}$ hydrogen plasma. See Data File: 21. (PPL-786358)
- Figure 14. Peak central ion temperature from charge exchange measurements as a function of injected beam power and target electron density. The appended numbers identify the experimental run corresponding to the tabulated (Appendix I) data base. (PPL-786394)
- Figure 15. Plot of the ion temperature increase normalized to beam power as a function of line average electron density at peak ion temperatures ($\bar{n}_e(P)$). (PPL-786379)
- Figure 16. Plot of ion temperature increase versus the ratio of beam power to line average electron density at peak ion temperature. (PPL-786376)
- Figure 17. Peak ion temperature as a function of P_B/\bar{n}_e . The pre-injection ion temperature corresponding to each data point is shown in the lower portion of the figure. Solid data points denote the onset of density fluctuations following peak ion temperature inferred from microwave interferometer density signals. (PPL-786467)
- Figure 18. Rise and fall times of the charge exchange ion temperature due to beam heating as a function of mean line average electron density, $\langle \bar{n}_e \rangle = (\bar{n}_e(I) + \bar{n}_e(P))/2$. (PPL-786468)
- Figure 19. Rise and fall times of the charge exchange ion temperature multiplied by the mean line average electron density plotted against peak ion temperature. (PPL-786463)
- Figure 20. Code generated profiles (neutral density and ion temperature) used in deducing the central ion temperature corrected for plasma profile effects. (PPL-786466)

Figure 21. Code simulated charge exchange energy distribution (upper plot) compared with the diagnostic results (lower plot). The code spectrum yields an apparent ion temperature of 3.6 keV from a fit between energy limits of 6.0 and 19.0 keV, as does the experimental spectrum. The actual central value given by the code correction is slightly higher: 3.7 keV. In the lower plot, the solid line corresponds to the code spectrum which is normalized to the data at an energy of $E = 19$ keV. (PPL-786465)

Figure 22. Rise and fall times of the charge exchange ion temperature plotted against the calculated stopping time, τ_{stop} . The curves drawn through the data points result from a linear least squares fit. (PPL-786464)

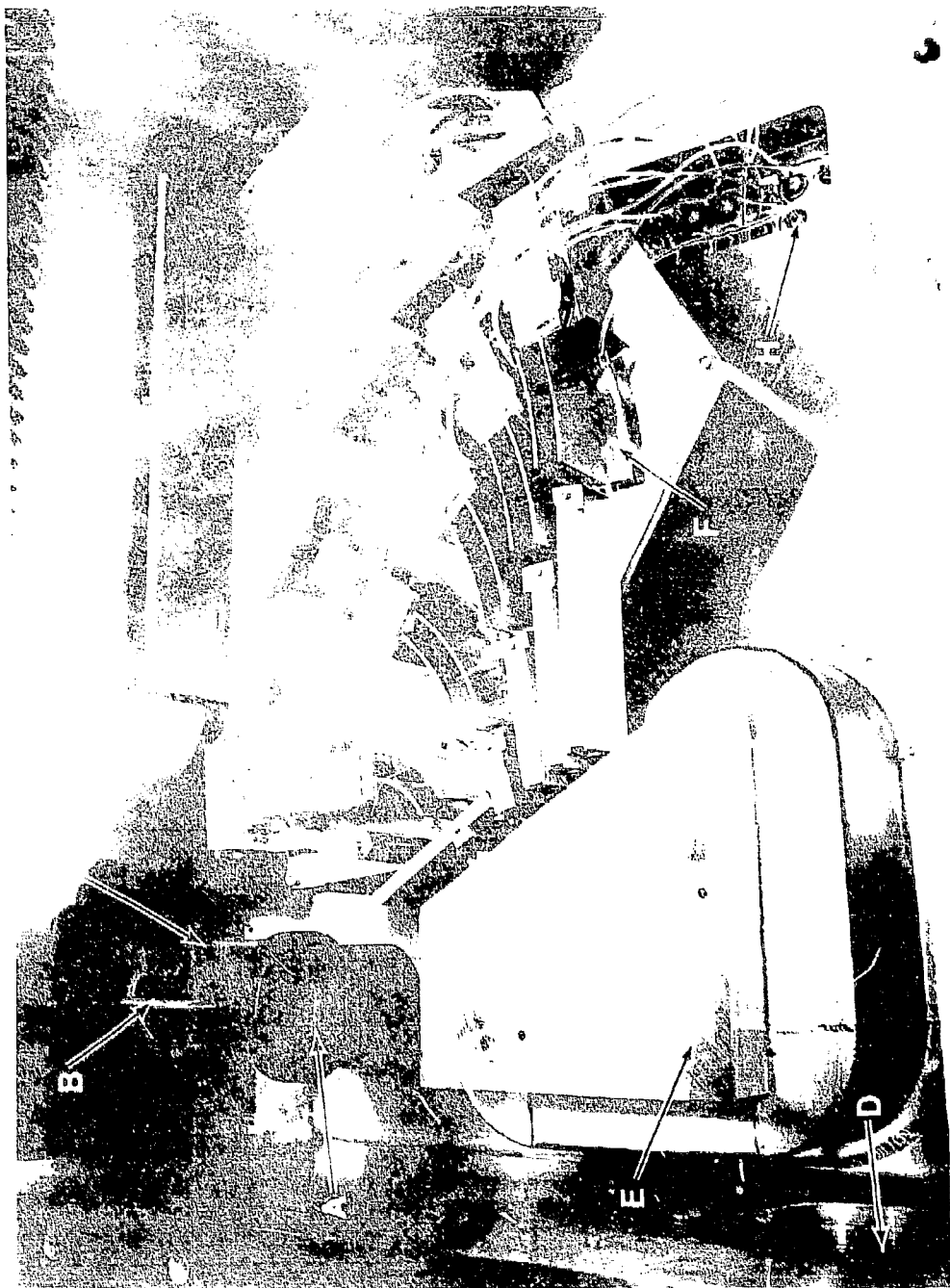


Fig. 1. 20647

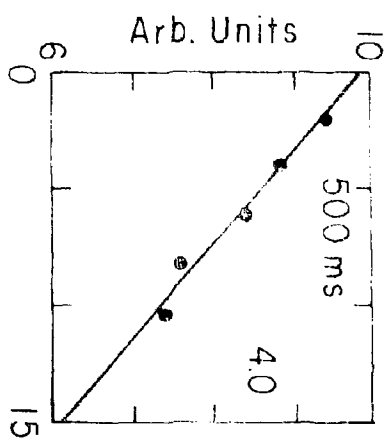
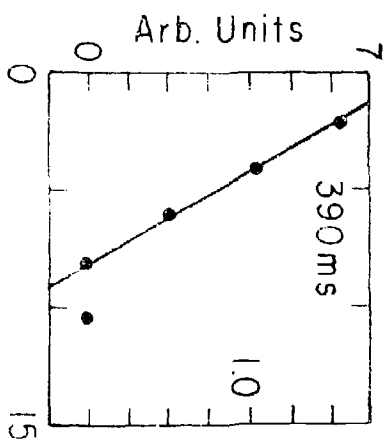
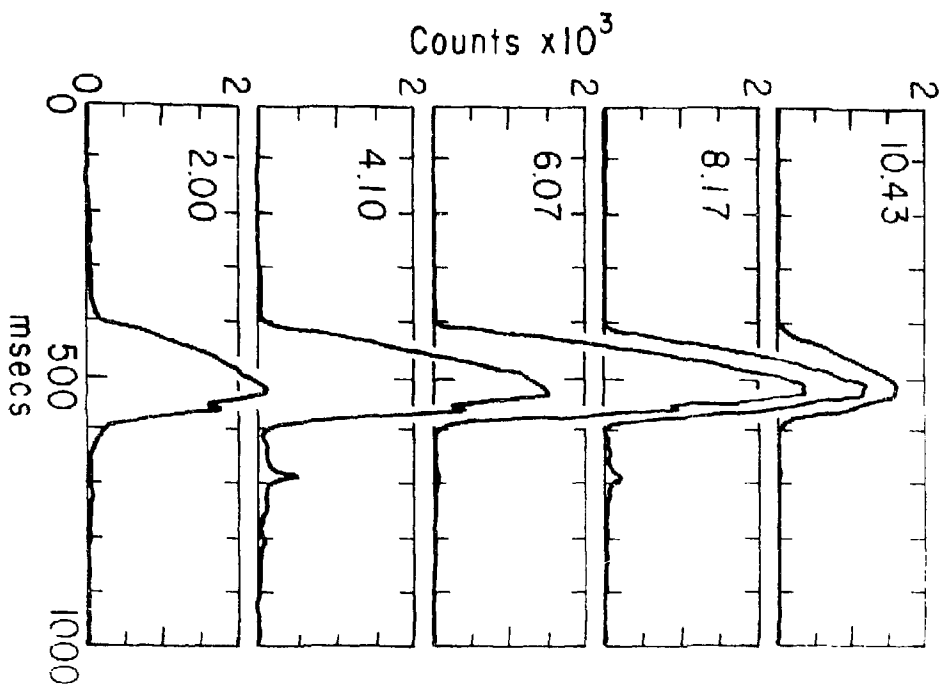


Fig. 2. /26073

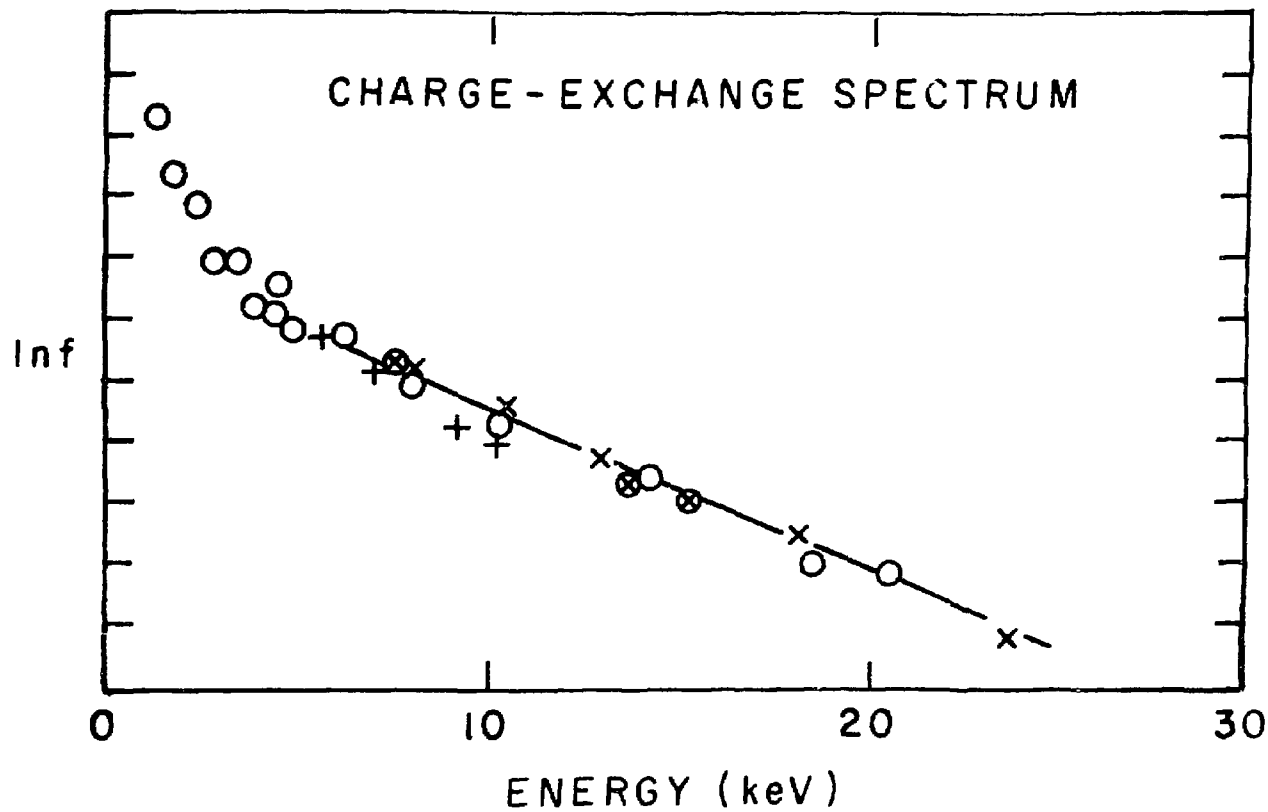


Fig. 3. 783883

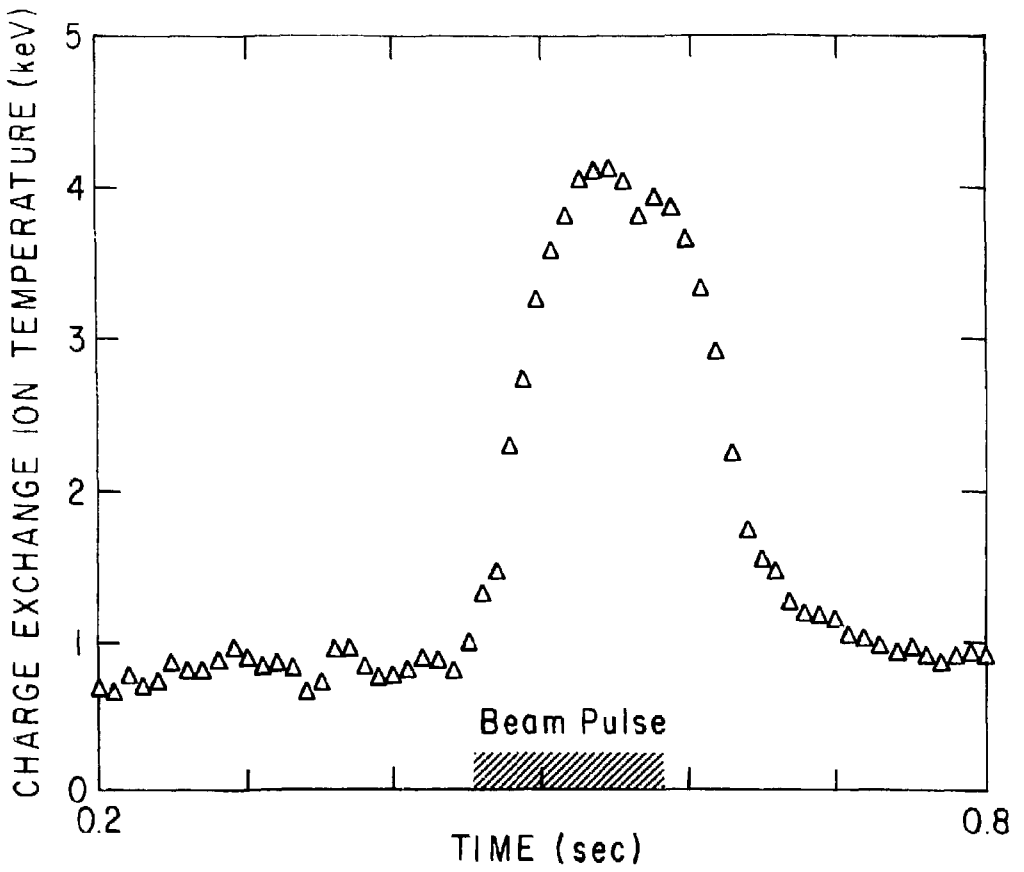


Fig. 4. 783872

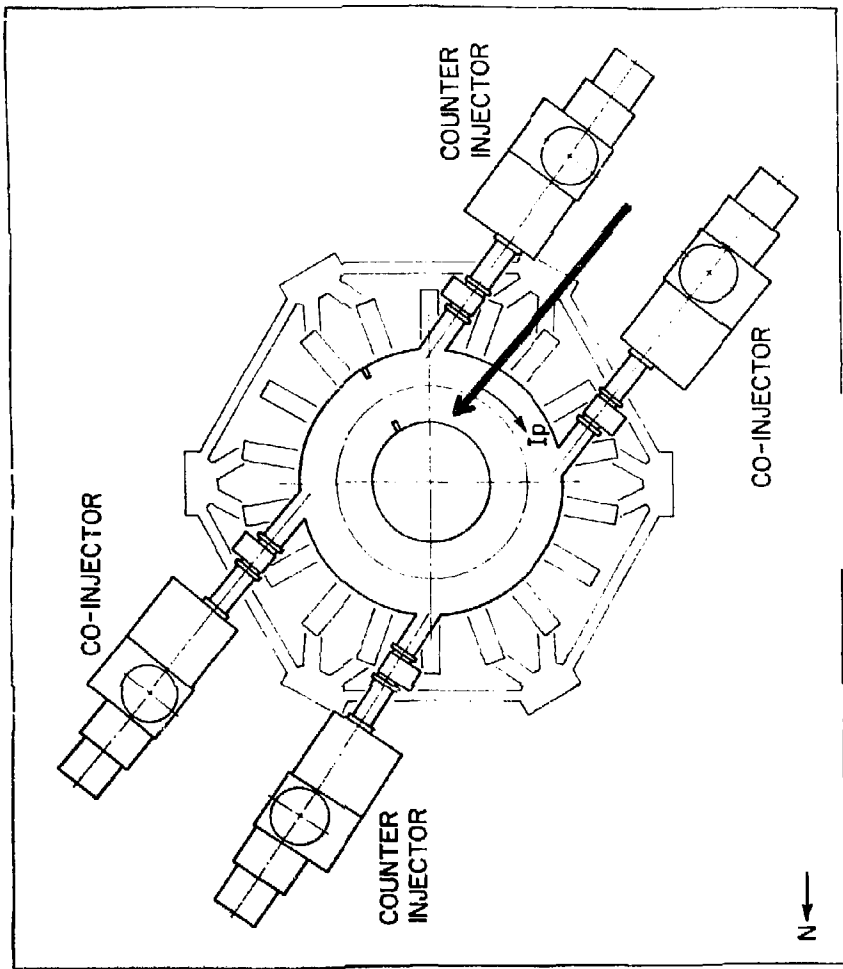


Fig. 5. 783851

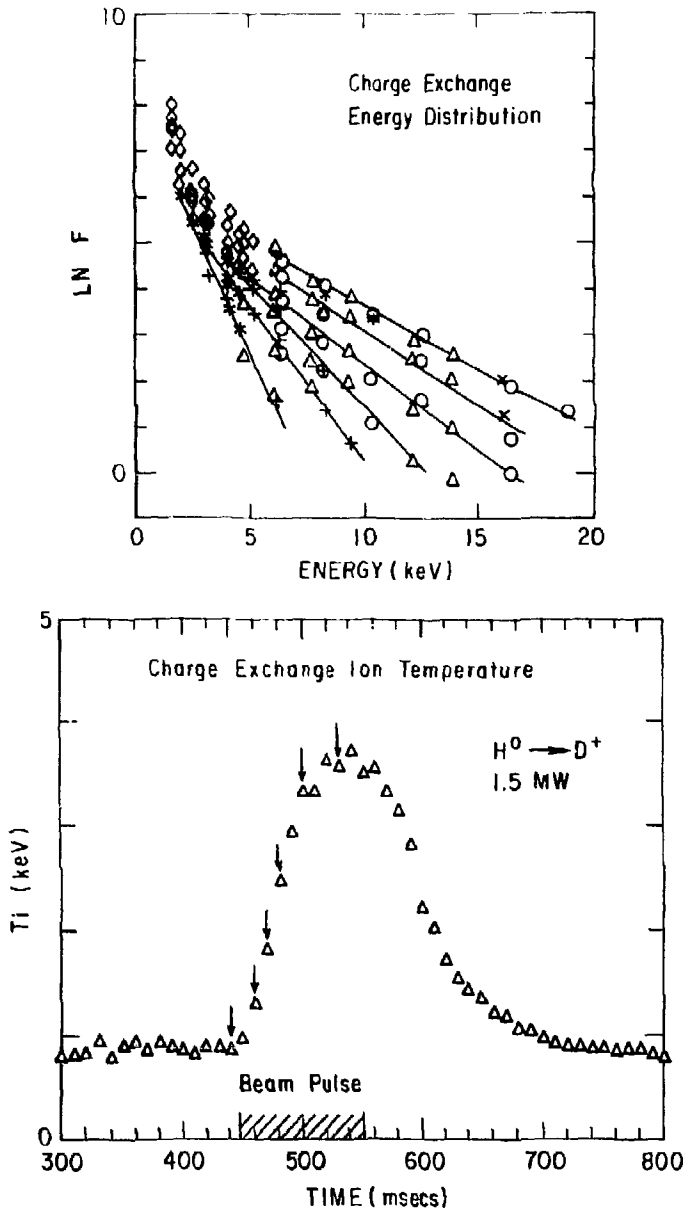


Fig. 6. (DATA FILE: 2) 786356

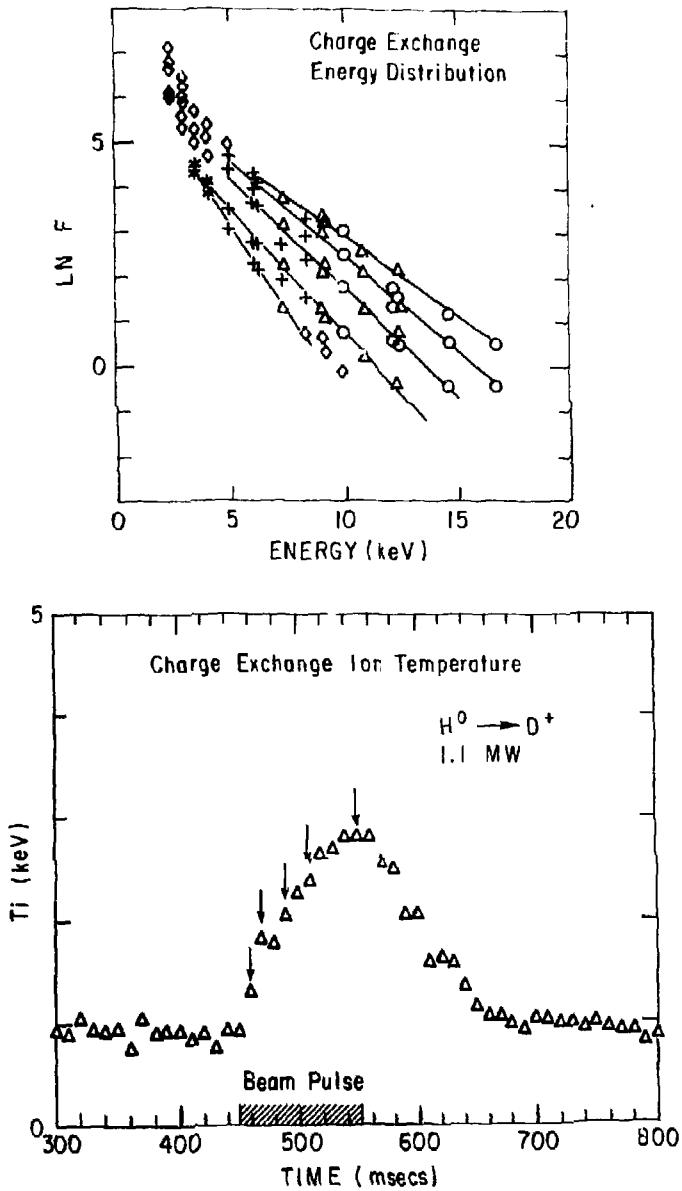


Fig. 7. (DATA FILE: 3) 786351

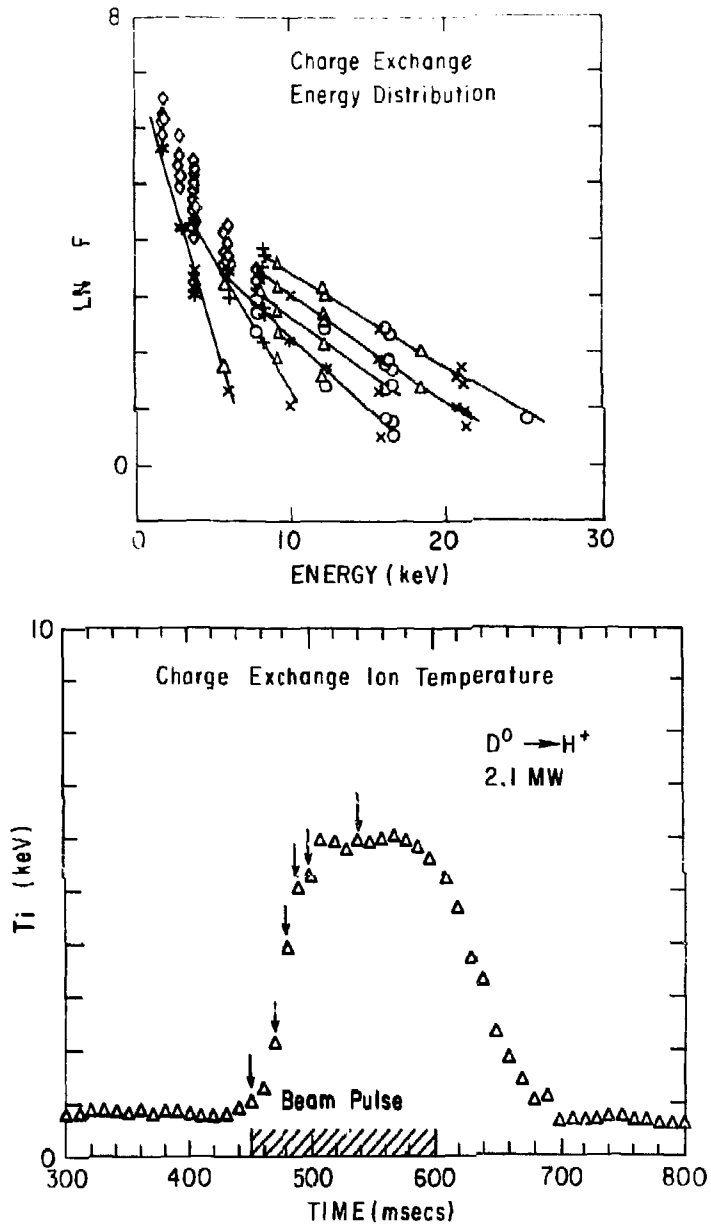


Fig. 8. (DATA FILE: 7) 786354

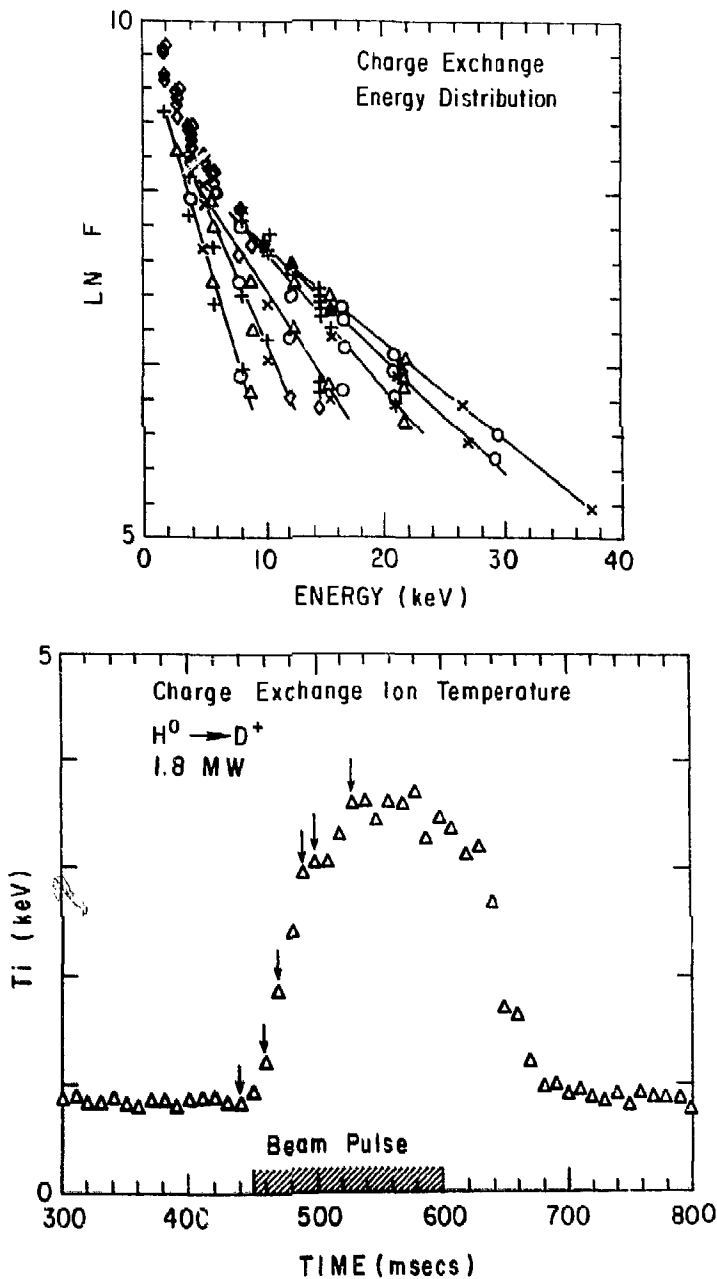


Fig. 9. (DATA FILE: 9) 786353

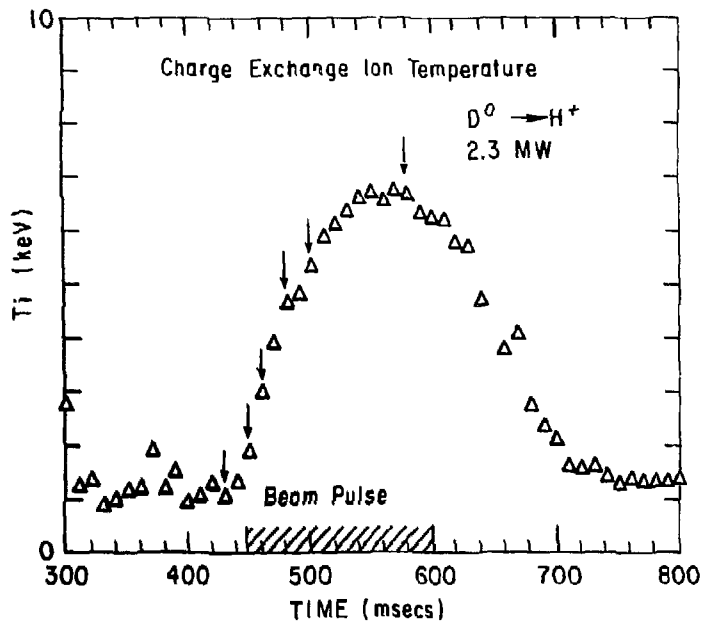
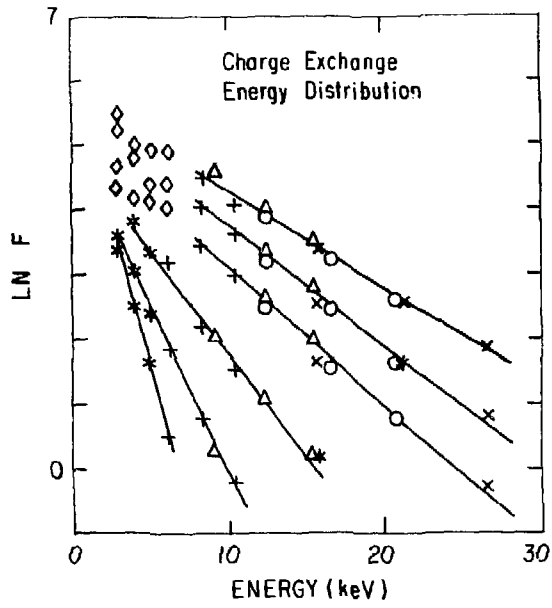


Fig. 10. (DATA FILE: 11) 786357

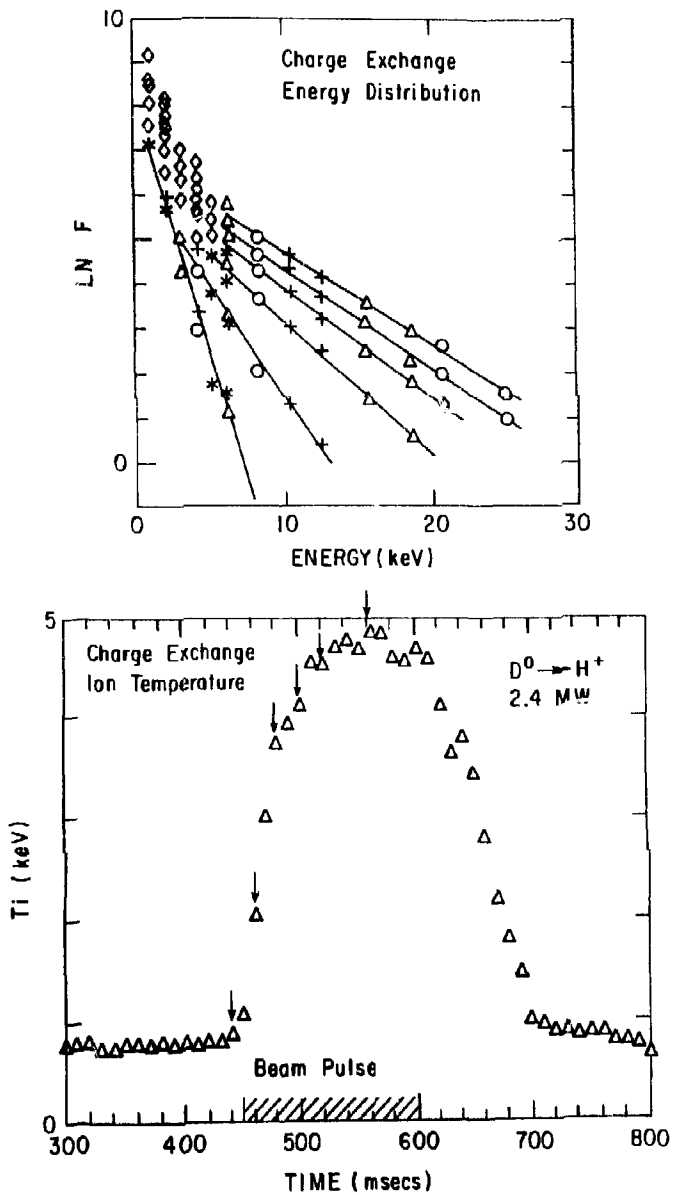


Fig. 11. (DATA FILE: 14) 786352

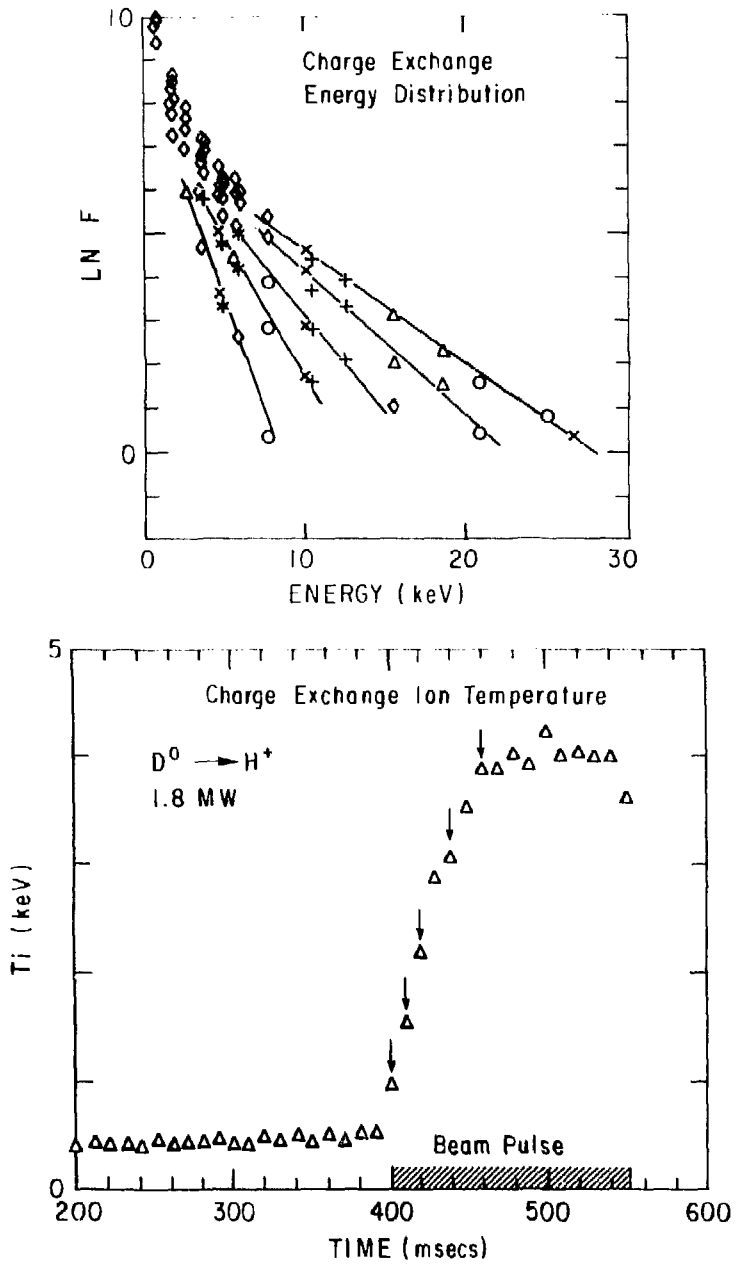


Fig. 12. (DATA FILE: 15) 786355

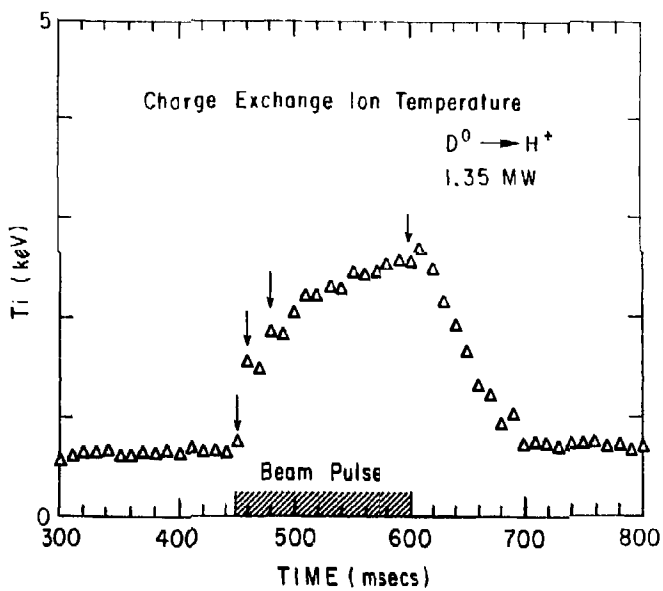
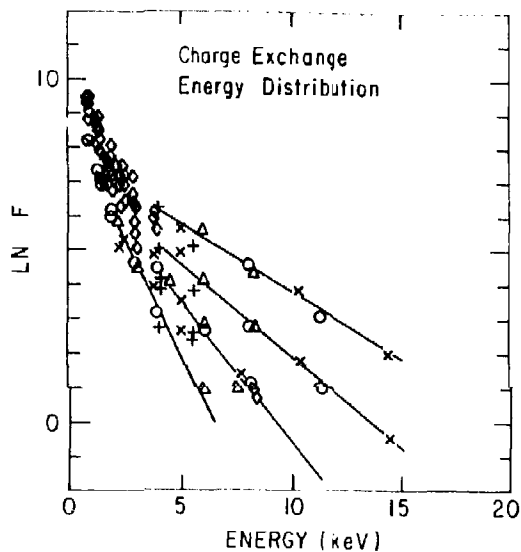


Fig. 13. (DATA FILE: 21) 786358

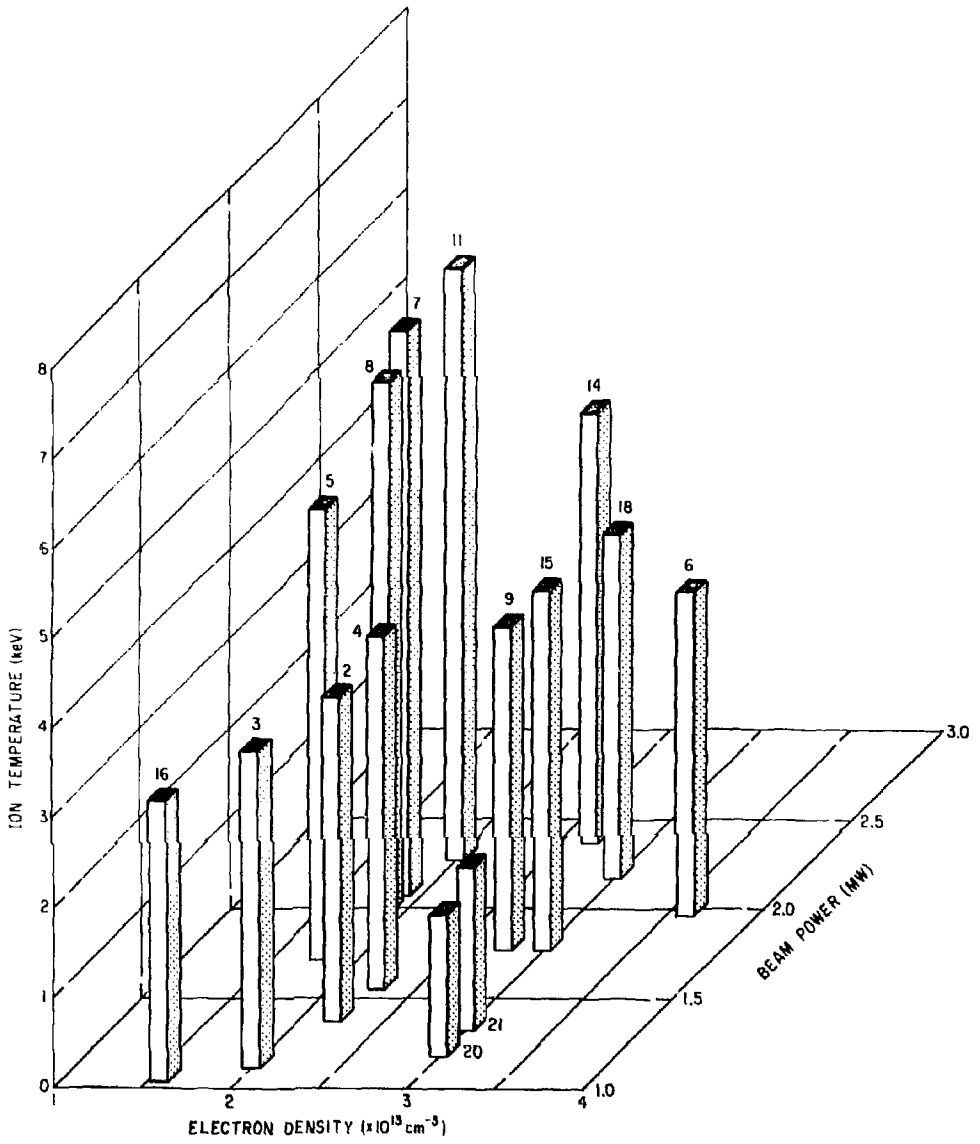


Fig. 14. 786394

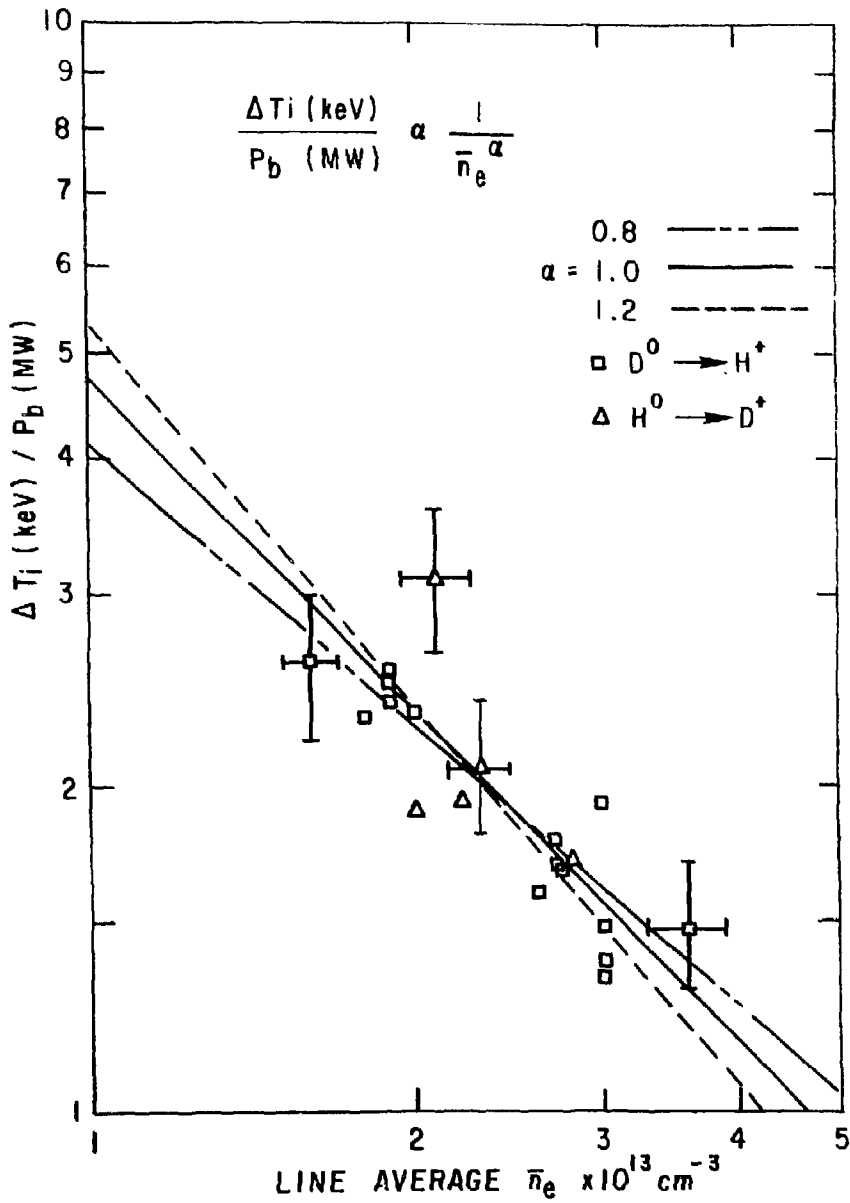


Fig. 15. 786379

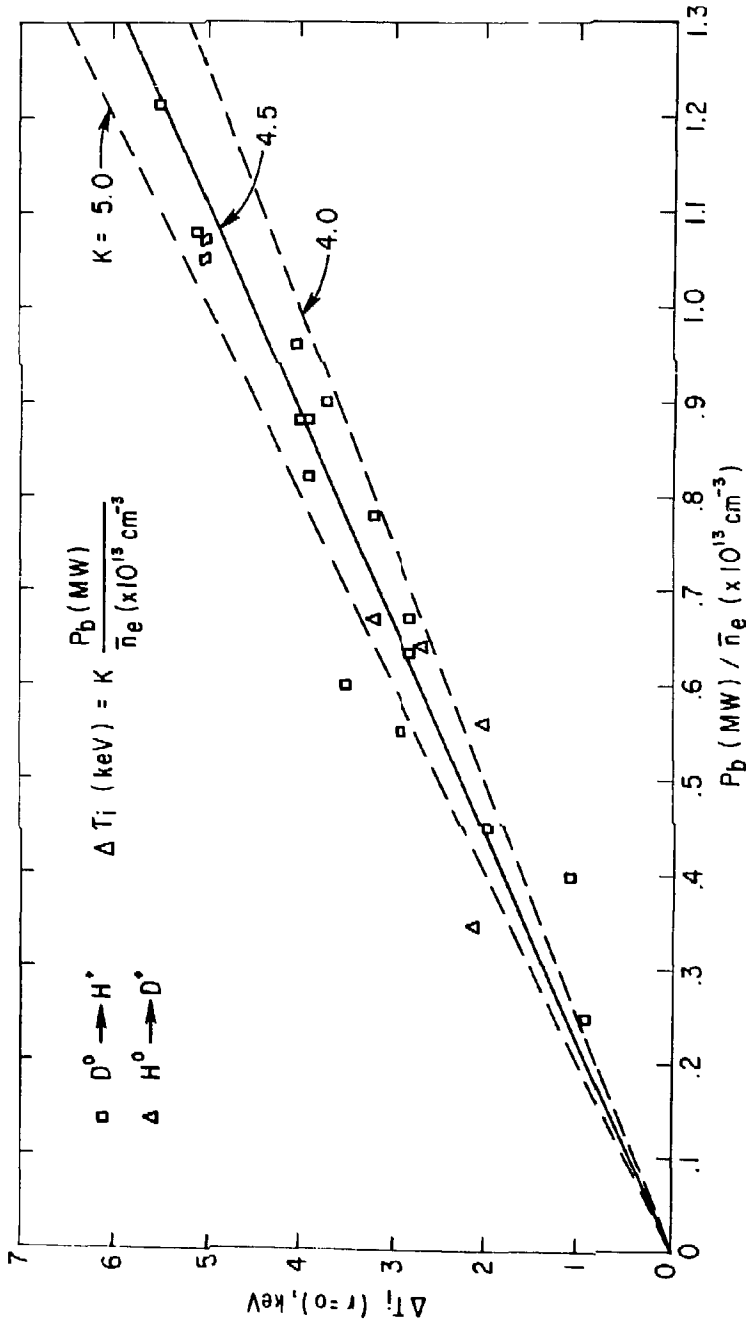


Fig. 16. 786376

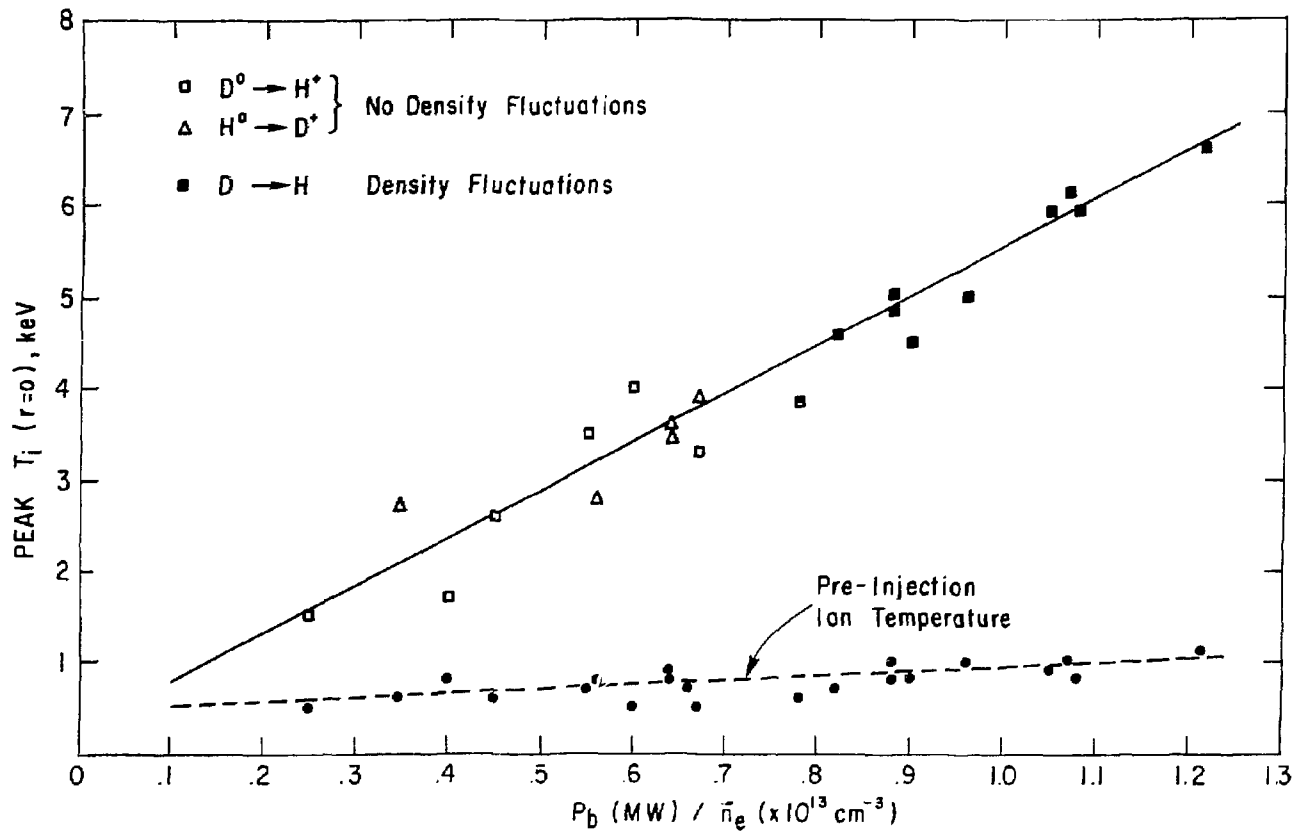


Fig. 17. 786467

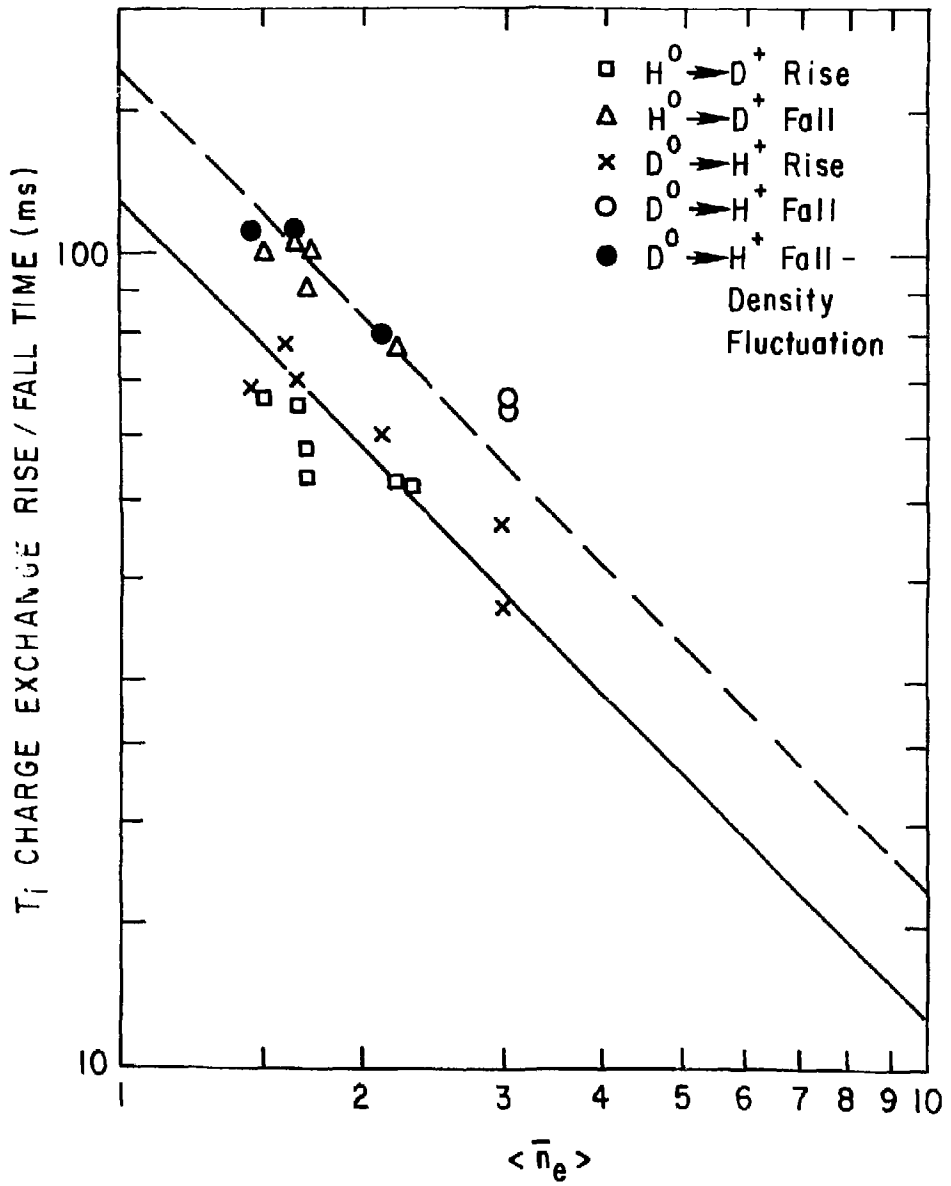


Fig. 18. 786468

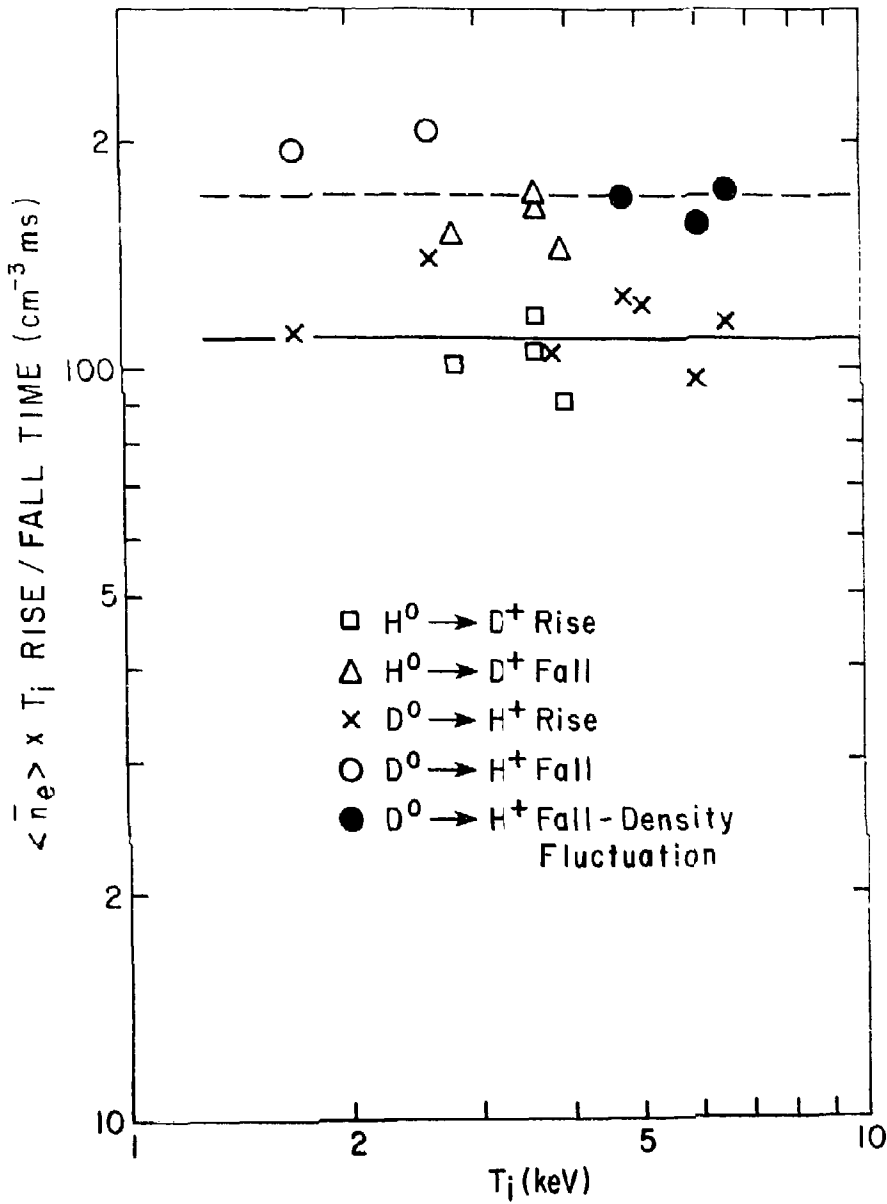


Fig. 19. 786463

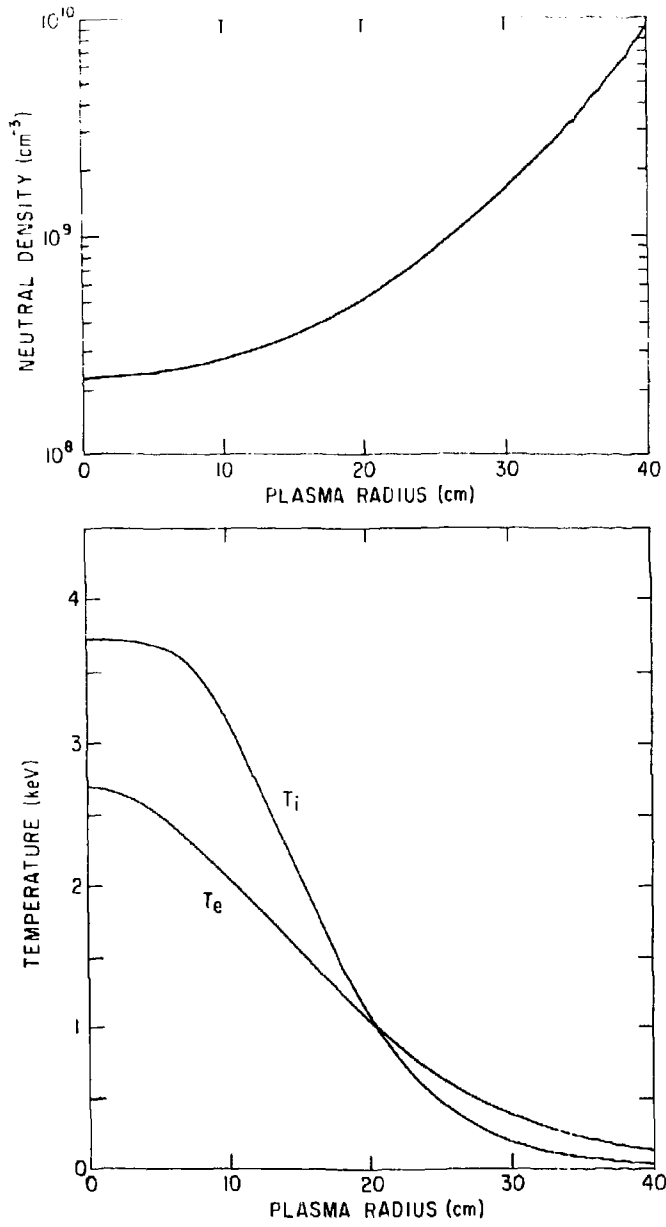


Fig. 20. 786466

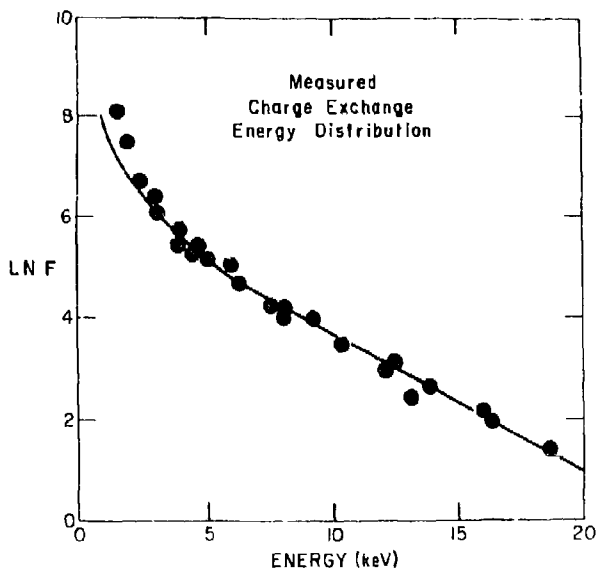
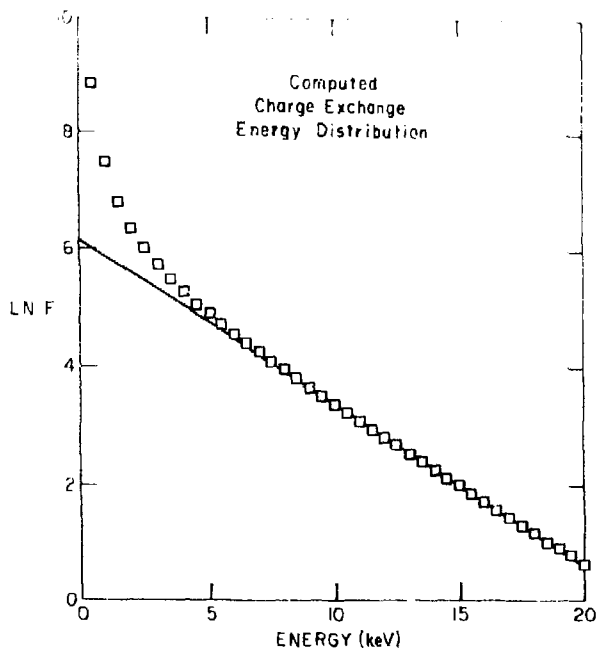


Fig. 21. 786465

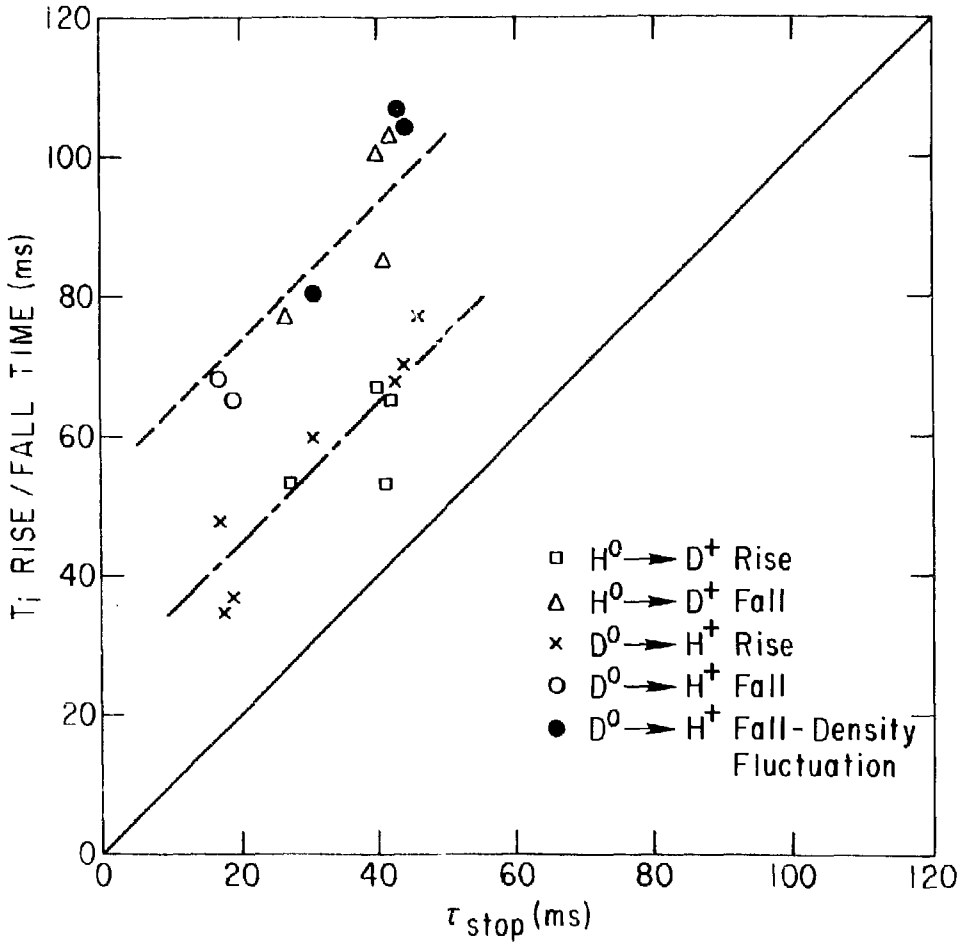


Fig. 22. 786464

THEORETICAL

- B. Anagnostopoulos, University, Australia
 S. T. Wu, University of Melbourne
 Geophysical Institute, Univ. of Alaska
 G. L. Johnston, Sonoma State Univ., California
 H. H. Kuehl, Univ. of So. California
 Institute for Energy Studies, Stanford University
 H. D. Campbell, University of Florida
 N. L. Olson, University of South Florida
 A. M. Stacey, Georgia Institute of Technology
 Benjamin M. Lawa State University
 Magne Kristiansen, Texas Tech. University
 W. L. Winters, Nat'l Bureau of Standards, Wash., D.C.
 Australian National University, Canberra
 C. N. Wainman-Munro, Univ. of Sydney, Australia
 E. C. G. Sudar, Inst. for Theo. Physics, Austria
 Louis Roy de Miltaine, Brussels, Belgium
 D. Paulinbo, Univ. of Tur. Comm., Belgium
 P.H. Saldanha, Instituto de Física, Campinas, Brazil
 C. P. Jovan, University of Alberta, Canada
 J. B. Bratton, INRS-Energie, Vancouver, Quebec
 H. H. Gungor, Univ. of Sakata de wati, Canada
 E. C. G. Sudar, Culham Laboratory, Abingdon, England
 M. D. Dapsis Library, C.E.N.-G, Grenoble, France
 Central Res. Inst. for Physics, Hungary
 K. Singal, Meerut College, India
 M. Naraghi, Atomic Energy Org. of Iran
 Biblioteca, Frascati, Italy
 Biblioteca, Milano, Italy
 G. Rostagni, Univ. Di Padova, Padova, Italy
 Project Library, Inst. de Física, Pisa, Italy
 Energy, Plasma Physics Lab., Gokasho, Uji, Japan
 S. Ohri, Japan Atomic Energy Res. Inst., Tokai-Mura
 Research Information Center, Nagoya Univ., Japan
 S. Shirota, Tokyo Inst. of Tech., Japan
 Inst. of Space & Aero. Sci., Univ. of Tokyo
 T. G. Onda, Univ. of Tokyo, Japan
 H. Yamato, Toshiba R. & D. Center, Japan
 M. Yoshikawa, JAERI, Tokai Res. Inst., Japan
 N. Yamana, Kyushu Univ., Japan
 R. England, Univ. Nacional Autónoma de México
 B. S. Liley, Univ. of Waikato, New Zealand
 S. A. Moss, Saab-Univers Norge, Norway
 I.A.C. Cabral, Univ. de Lisboa, Portugal
 O. Petrus, A.L.I. CUGA Univ., Romania
 J. de Villiers, Atomic Energy Bd., South Africa
 A. Maurech, Comisaría De La Energy y Recursos
 Minerales, Spain
 Library, Royal Institute of Technology, Sweden
 Cen. de Res. En Phys.Des Plasmas, Switzerland
 Librarian, Fom-Instituut Voor Plasma-Fysica, The
 Netherlands
 V. E. Golant, A.F. Ioffe Physical-Tech. Inst., USSR
 B.B. Kadomtsev, Kurchatov Inst. of Atomic Energy,
 USSR
 The Kharkov Physical-Tech. Inst., USSR
 M. S. Rabinovich, Academy of Sci, USSR
 Bibliothek, Stuttgart, West Germany
 R.D. Buhler, Univ. of Stuttgart, West Germany
 Max-Planck-Inst. für Plasmaphysik, W. Germany
 Nucl. Res. Estab., Jülich, West Germany
 K. Schindler, Inst. Für Theo. Physik, W. Germany

EXPERIMENTAL
THEORETICAL

- M. H. Brennan, The Univ. of Oz., Australia
 H. Barnard, Univ. of British Columbia, Canada
 S. Sreenivasan, Univ. of Calgary, Canada
 T. Paret, C.E.N.-B.P., Fontenay-aux-Roses, France
 Prof. Schatzman, Observatoire de Nice, France
 S. C. Sharma, Univ. of Cape Coast, Ghana
 R. N. Aiyer, Laser Section, India
 B. Buti, Physical Res. Lab., India
 L. K. Chavda, S. Gujarat Univ., India
 I.M. Das Das, Banarus Hindu Univ., India
 S. Coperman, Tel Aviv Univ., Israel
 E. Greenspan, Nuc. Res. Center, Israel
 P. Rosenau, Israel Inst. of Tech., Israel
 INF Center for Theo. Physics, Trieste, Italy
 I. Kawakami, Nihon University, Japan
 T. Nakayama, Ritsumeikan Univ., Japan
 S. Nagao, Tohoku Univ., Japan
 T.I. Sakai, Toyama Univ., Japan
 S. Tjøtta, Univ. i Bergen, Norway
 M.A. Hellberg, Univ. of Natal, South Africa
 H. Wilhelmson, Chalmers Univ. of Tech., Sweden
 Astro. Inst., Sonnenborn Obs., The Netherlands
 N.G. Tsintsadze, Academy of Sci USSR, USSR
 T. J. Boyd, Univ. College of North Wales
 K. Hubner, Univ. Heidelberg, W. Germany
 H. J. Kaeppler, Univ. of Stuttgart, West Germany
 K. H. Spatschek, Univ. Essen, West Germany

EXPERIMENTAL
ENGINEERING

- B. Grik, Univ. de Quebec, Canada
 P. Lukar, Komenského Univ. of Trnava, Slovakia
 G. Horikoshi, Nat'l Lab for High Energy Physics,
 Tsukuba-City, Japan
 V. A. Galukhki, D.V. Uremov Sci.
 Res. Institut of Elect. App., USSR

EXPERIMENTAL

- F. J. Paulson, Univ. of Wollongong, Australia
 T. Kistemaker, Fom Inst. for Atomic
 & Molec. Physics, The Netherlands

THEORETICAL

- F. Verheest, Inst. Vor Theo. Mech., Belgium
 J. Teichmann, Univ. of Montreal, Canada
 T. Kahan, Univ. Paris VII, France
 R. K. Chhajlani, India
 S. K. Trehan, Punjab Univ., India
 T. Namikawa, Osaka City Univ., Japan
 H. Narumi, Univ. of Hiroshima, Japan
 Korea Atomic Energy Res. Inst., Korea
 E. T. Karlson, Uppsala Univ., Sweden
 L. Stenflo, Univ. of UMEA, Sweden
 J. R. Sarai, New Univ., United Kingdom